

From the Outside in: An Overview of Positron Imaging of Plant and Soil Processes

Michael P. Schmidt¹ , Steven D. Mamet¹, Richard A. Ferrieri², Derek Peak¹, and Steven D. Siciliano¹

Abstract

Positron-emitting nuclides have long been used as imaging agents in medical science to spatially trace processes non-invasively, allowing for real-time molecular imaging using low tracer concentrations. This ability to non-destructively visualize processes in real time also makes positron imaging uniquely suitable for probing various processes in plants and porous environmental media, such as soils and sediments. Here, we provide an overview of historical and current applications of positron imaging in environmental research. We highlight plant physiological research, where positron imaging has been used extensively to image dynamics of macronutrients, signalling molecules, trace elements, and contaminant metals under various conditions and perturbations. We describe how positron imaging is used in porous soils and sediments to visualize transport, flow, and microbial metabolic processes. We also address the interface between positron imaging and other imaging approaches, and present accompanying chemical analysis of labelled compounds for reviewed topics, highlighting the bridge between positron imaging and complementary techniques across scales. Finally, we discuss possible future applications of positron imaging and its potential as a nexus of interdisciplinary biogeochemical research.

Keywords

PET imaging, FDG, autoradiography

Introduction

The first documented use of a positron emitting tracer in a biological system was from 1939, where Samuel Rubin and colleagues from the University of California applied [¹¹C]CO₂ produced from bombardment of ¹¹B with deuterons by one of Lawrence's cyclotrons to barley plants under different lighting treatments.¹ [¹¹C]CO₂, traced by ¹¹C, was fixed by barley (*Hordeum vulgare*) and followed into chemically extractable fractions of plant material, allowing for assessment of plant metabolic partitioning of recent photoassimilates (i.e. carbon-containing compounds from fixed CO₂ conversion by photosynthesis) into different fractions (e.g., water soluble carbohydrates, pigments, insoluble materials). This study showed the potential to use ¹¹C for quantitative determination of carbon fixation by plants, but also its fate within subject plants.

Despite foundational work in the late 1930s with positron-emitting tracers in plants, it was not until 1988 that positron imaging was first applied to plant processes.² In that study, McKay and colleagues at Queen's University in Canada used positron emission tomography (PET) to image the *in vivo*

uptake and transport of [¹⁸F]fluoride ion ([¹⁸F]F⁻) as a probe for water dynamics in soybeans (*Glycine max*). Through rapid imaging and high spatial resolution (≈4 mm), PET was used to quantitatively assess the extent of tracer flow within the plant, tracer binding to the plant, and tracer flow speed and volume. Although the authors stated that other approaches could obtain these data with "comparable or greater accuracy," they concluded that, "the capability of the PET method to provide these characteristics on a regional basis with relatively high spatial and temporal resolution has no parallel."²

¹ Department of Soil Science, College of Agriculture and Bioresources, University of Saskatchewan, Saskatoon, Canada

² Interdisciplinary Plant Group, Division of Plant Sciences, Department of Chemistry, Missouri Research Reactor Center, University of Missouri, Columbia, MO, USA

Submitted: 25/10/2019. Revised: 14/09/2020. Accepted: 17/09/2020.

Corresponding Author:

Michael P. Schmidt, Department of Soil Science, University of Saskatchewan, 51 Campus Drive, Saskatoon, Saskatchewan, Canada S7N 5A8.
Email: mps286@usask.ca



Creative Commons Non Commercial CC BY-NC: This article is distributed under the terms of the Creative Commons Attribution-NonCommercial 4.0 License (<https://creativecommons.org/licenses/by-nc/4.0/>) which permits non-commercial use, reproduction and distribution of the work without further permission provided the original work is attributed as specified on the SAGE and Open Access pages (<https://us.sagepub.com/en-us/nam/open-access-at-sage>).

Since this benchmark study, the use of PET and other positron-imaging approaches, such as positron radiography and the positron emitting tracer imaging system (PETIS), have greatly expanded in environmental sciences.³ While these imaging modalities all spatially visualize positron emitting nuclide distribution, they operate on different principles and provide distinct spatial as well as temporal viewpoints on tracer distribution. PET and PETIS both spatially trace positron emitting nuclides through antiparallel emission (approximately 180°) of paired gamma rays from the point of annihilation with an electron, usually within a few millimeters of positron emitting nuclide decay.⁴ With PET, emitted gamma rays are detected by an array of scintillator crystal detector blocks arranged in a ring, or stack of rings. Paired detectors approximate the location of annihilation events by simultaneously detecting the coincidence trajectory of emitted gamma rays in the plane of detectors.^{4,5} After considerable post-processing of raw coincidence counts from detectors, 3-dimensional and time-resolved distribution of positron emitting nuclides in subjects placed within the detector array may be obtained.⁵ Typically, tracer distribution with PET is expected to have a spatial resolution of a few millimeters due to positron travel before annihilation. For a more detailed description of the history, physics, instrumentation, and data processing associated with PET, see references 6 and 7.^{6,7} PETIS imaging is similar to PET in that it traces positron annihilation events, but notable a notable discrepancy in detection systems results in different imaging capability.³ PETIS imaging is based on a single pair of detector sets, rather than an array of detectors employed in PET. Samples (within an environmental context, PETIS has been applied only to plant samples thus far) are placed equidistant between paired detectors and perpendicular to the detector faces. The assumption of equidistance from detection defines the plane from which gamma rays may be emitted, allowing for determination of isotope tracer from an individual annihilation occurrence. This benefit allows researchers to visualize radionuclide distribution in real-time, as it bypasses post-hoc reconstruction required to delineate tracer distribution in PET images. There are some limitations associated with PETIS imaging, however. Due to the inherent need for sample placement along a plane perpendicular to detectors, PETIS is restricted to 2-dimensional dimensional imaging, unlike PET which can yield 3-dimensional distributions. Additionally, samples need to be able to conform to a thin, planar orientation, which may restrict applicability. For a more detailed discussion of the history and progression of PETIS imaging systems, the reader is directed to a recent textbook chapter outlining PETIS in greater detail.³

Radiography differs from PET and PETIS in several ways, including the detection of emitted positrons rather than annihilation photons and greater spatial resolution (roughly 50-100 μm for radiography versus a few mm for PET).⁸ Radiographic imaging is also restricted to 2-dimensional imaging, unlike PET. To achieve optimum resolution with radiographic imaging, intimate contact between samples and the imaging film or plate is necessary, which needs to be considered for radiographic imaging experiments. Real-time imaging is generally

Table 1. Range of Some Positrons Commonly Used in Plant Studies.^a

Isotope	R _{max} (mm)	R _{mean} (mm)
¹¹ C	4.2	1.2
¹³ N	5.5	1.8
¹⁵ O	8.4	3.0
¹⁸ F	2.4	0.6
⁶⁴ Cu	2.5	0.7

^aR_{max} and R_{mean} represent maximum and mean ranges in water, respectively.

not accessible with radiographic imaging due to the development of radiographic plates and films. A series of images may be acquired with radiographic imaging, however, yielding a time series of tracer distribution images. Together, these benefits and drawbacks provide a different approach to imaging positron emitting nuclides from PET and PETIS, giving researchers access to fundamentally different imaging capabilities when designing experiments.

Expanded use of radiographic imaging and PET in environmental science has largely been driven by use in plant studies. Other fields, such as geological and soil sciences, have also been using PET since the 1990s as well. In this review, we (i) summarize these applications of positron imaging in environmental systems and briefly describe experimental outcomes accessible with positron imaging, (ii) highlight the interface between positron imaging and other imaging and chemical analyses in these studies, where applicable, and (iii) outline the future potential of positron imaging modalities as a key nexus in environmental systems to address pressing issues in biogeochemistry and agriculture.

Physics of Positron Detection in Plant and Soil Systems

Detection of positrons in plants can be challenging given the distance of positron movement before annihilation (several millimeters) and the inherently thin nature of plant tissues, which allows for positron escape before annihilation (Table 1).⁹ Hence, there is a discrepancy between the point of positron emission and where annihilation gamma rays originate. The spatial discrepancy is a particularly important consideration for PET detection in plants. Incorporating known emission locations, such as a major vein or root and known density gradients, e.g. soil versus tissue, is an essential component when interpreting PET derived images. In contrast, radiographic imaging is susceptible to positron attenuation effects, which could skew images in thicker plant tissues. For example, [¹⁸F]F⁻ distribution in a tobacco leaf by radiographic and PET imaging demonstrates the conflicting results imaging approaches may yield due to the nature of detection of radioactive decay (positrons versus gamma rays) and the nature and density of the biological medium in which the radioisotope occupies (Figure 1). Autoradiographic imaging plates contain crystals that are ionized by beta radiation (e.g. positrons), but gamma rays have a much lower probability of exciting a phosphor plate crystal. Thus,

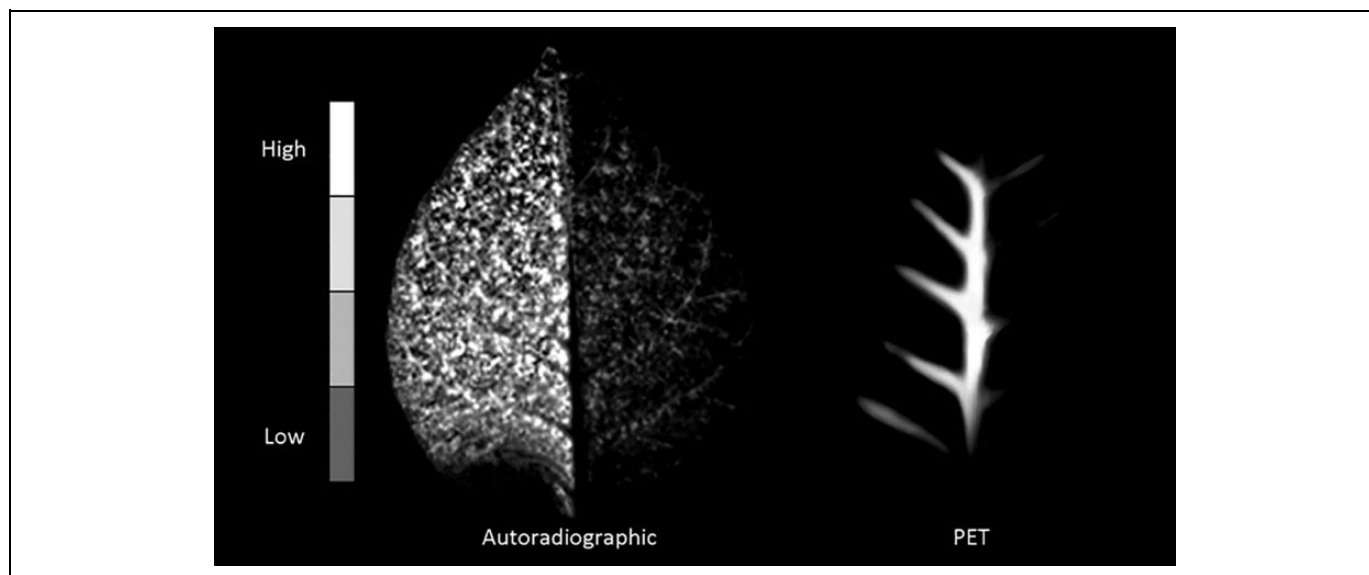


Figure 1. Leaf uptake and distribution of $[^{18}\text{F}]\text{F}^-$ imaged by autoradiography and PET. The images differ because autoradiography (left) detects escaped positrons (from decays that occur within the positron's range of the plate), but because those escaped positrons annihilate outside the thinner, non-vascular leaf tissues they are not imaged by PET (right). The PET image, however, preferentially highlights tracer abundance within vascular tissue where positron annihilation occurs before positrons escape from these thicker structures. In both cases of imaging, the right side of an intact tobacco leaf from different plants is shaded causing more tracer to transport to the left-side.

positrons that escape the plant are detected by the phosphor plate, while gamma rays are effectively not detected by the phosphor plate, resulting in a lower quality image.¹⁰

The range has a probability distribution, with a maximum value: mean and maximum ranges of relevant nuclides in water are given in Table 1. For instance, positrons from ^{18}F decay have a lower range in bone tissue (density $\approx 1.92 \text{ g cm}^{-3}$, range $\approx 0.37 \text{ mm}$), compared to water (density $\approx 1.00 \text{ g cm}^{-3}$, range $\approx 0.62 \text{ mm}$).¹¹ Hence, when using autoradiography, the density of the material directly influences the ability to detect the radioactivity. Thus, the leaf image on the left of Figure 1 was corrected for tissue density of the veins and the distance of the veins from the detector using the probability distribution for positron annihilation as a function of density.¹¹ Vein distance from the leaf edge was 206, 88, and 67 μm for midvein, secondary, and tertiary, respectively, and the positron correction factors for veins ranged from 3 to 25%, depending on the vein type. The positron annihilation dependence on density and distance, explains why the PET image, which only detects gamma rays released upon annihilation, differs from the radiographic image. Only the midvein at 206 μm had enough distance and density to cause enough positrons to annihilate and thereby produce the coincidental gamma rays sensed by the PET detectors.

Like autoradiography, PET detection systems are sensitive to distance and density effects on positrons and photons.¹² The overall uncertainty caused by material density can be thought of as arising from 2 classes of uncertainty: (i) attenuation and (ii) detector physics. Gamma ray attenuation arises as a function of the Lambert-Beer law in which the intensity declines as a function of distance and electron density along the line

through which the gamma ray passes. Attenuation consists of photoelectric absorption, pair production, Rayleigh scattering, and Compton scattering. Compton scatter is the dominant attenuation process and can affect up to 70% of all detected photons in PET.¹³ The effect of Compton scattering on image reconstruction can be minimized by using a smaller energy window of the detected photons. For example, a large energy window detected twice as many scattered photons over a 100 mm range compared to the unscattered photons, which in turn only had a 50 mm longitudinal window.¹⁴ Detector physics refers to the design of the detection system to minimize photon non-collinearity and photon detector element. Photon non-collinearity arises because photons are not always emitted at 180 degrees apart if the positron and electron are not at rest when combined. Non-collinearity can be minimized by decreasing the detection system diameter and, similarly, smaller photon detector elements that act more effectively over shorter coincidence times, minimize the effects of attenuation, scattering, and non-collinearity effects.¹³ In the context of positron imaging applied to environmental systems, non-collinearity and density effects may be important to consider when designing an imaging experiment. For example, in soils and geomedias, the higher density materials likely to be used in PET imaging experiments will likely result in greater spatial resolution through a shorter positron trajectory length compared with plant tissues.¹⁴ These media, however, may favor greater attenuation and scattering of emitted photons relative to plant tissues. This may result in greater photon loss due to attenuation and scattering before detection relative to plants, where positron escape is a greater concern. For a recent detailed discussion of these considerations in PET imaging of

geomechanics the reader is referred to Zahasky et al.¹⁵ and Hubeau et al.,¹⁶ who provide an excellent outline of how PET and autoradiography differ when assessing plant tissues. Two chapters from a recent textbook on phloem research methods may be of further interest as they provide additional detail regarding imaging considerations in plant systems.^{17,18}

Advances in instrumentation and methodology have enhanced the ability to detect positrons throughout plant specimens despite the aforementioned methodological limitations (Figure 2).^{3,19,20} Along with (i) concurrent stable isotope application, (ii) chemical analyses (e.g., high performance liquid chromatography [HPLC]²¹), and (iii) imaging analyses (e.g., MRI and optical projection tomography [OPT]^{22,23}), positron imaging has proven to be a valuable tool for linking large-scale spatial relationships with molecular-level speciation.

The value of positron imaging to probing plants has been further bolstered through the suite of positron-emitting nuclides available to researchers in plant sciences. Table 2 lists isotopes used in imaging studies, along with corresponding half-lives and chemical forms. Using downstream chemical synthesis procedures to integrate positron emitting nuclides into allows for further tailoring of radionuclides to processes of interest, such as synthesis of 2-[¹⁸F]fluoro-2-deoxy-D-glucose ([¹⁸F]FDG) from [¹⁸F]F⁻ or ¹¹C-tagged molecules from [¹¹C]CO₂. Additionally, metal radionuclides can be complexed by various ligands, allowing for the modification of the local chemical environment of some positron-emitting metals.

The relatively short half-lives of many positron emitting nuclides, particularly ¹¹C, ¹³N, ¹⁵O, and ¹⁸F affords unique capabilities, as well. This includes the ability to make repeated radionuclide application on the same subject, either with the same or another label, which is particularly relevant when considering plant responses to treatments, changes in environmental variables, or other perturbations. Repeated application, thus, makes mechanistic studies more accessible with positron emitting nuclides than with stable isotopes with much longer half-lives (e.g., ¹⁴C, ¹⁵N), especially when probing rapid processes. An example of this is work by Ferrieri et al., wherein repeated doses of a [¹³N]NO₃⁻ tracer was used as a tracer in a study of NO₃⁻ uptake and translocation under nitrogen deprivation in a poplar sapling.²⁴ Alternatively, for processes with time scales that exceed the half-life of applied tracers, positron emitting nuclides may have limited applicability. In these situations, relevant stable isotopes should be considered more viable tracers. Therefore, if a dynamic process that alters tracer distribution in less than 10 half-lives of time, is of interest, then positron emitting nuclides may be appropriate. In contrast, a process with longer term effect is likely best evaluated using either longer-lived nuclides or stable nuclides.

The application of positron imaging to plant studies has increased significantly since the initial water transport analyses by McKay et al.² While dynamics of water movement with PET in plants has been widely studied,²⁵⁻³⁵ other topics related to PET have increasingly been investigated, including uptake and translocation of nutrients,^{36-52,98,99} photoassimilate fixation/allocation,^{15,22,23,53-80} sugar transport,^{21,82-87} and heavy

metal contaminant uptake and transport^{25,88-96,100} (Table 3). Many agriculturally important plant species have been used as study subjects in these investigations, such as maize, rice, and barley. Other studies, however, focus on processes of woody tree species, grasses, and ferns. Thus, positron imaging is suitable to a wide array of critical processes in plants within managed and natural systems. Applications of positron imaging to this diverse research base within plant sciences are presented here, highlighting the role of positron imaging work in understanding plant physiology and plant interaction with their environment.

Positron Imaging to Monitor Water Dynamics in Plants

Tracers Used for Monitoring Water Uptake and Translocation in Plants

Many studies on positron imaging in plant sciences have focused on plant uptake and translocation of water. The most commonly used radionuclide tracers in these studies were [¹⁸F]F⁻ and [¹⁵O]H₂O, representing chemical and radioactive analogues of water behavior in plant tissues (Table 2). Though [¹⁸F]F⁻ and [¹⁵O]H₂O have been used as tracers for water movement in plants, the 2 labels have key differences. For instance, [¹⁸F]F⁻ (110 minutes) has the benefit of a longer associated half-life than [¹⁵O]H₂O (122 seconds), allowing for imaging over longer periods of time. In addition, there are also differences in uptake and movement of [¹⁸F]F⁻ and [¹⁵O]H₂O, which Nakanishi et al.³¹ investigated in a soybean plant. They demonstrated that the ¹⁸F⁻ ion was taken up and translocated within soybean quicker than [¹⁵O]H₂O (Figure 3A). This indicates that [¹⁸F]F⁻ movement may not be an ideal tracer for water movement, unlike [¹⁵O]H₂O. However, [¹⁸F]F⁻ has many qualities of a good tracer for water flow in plants, including low required concentration, low binding to plant tissue, and xylem-mediated flow.² Another critical point when considering an appropriate tracer for water movement in plant studies is the nature of the transport process being studied (i.e. convective or diffusive flow). For example [¹⁵O]H₂O might be expected to diffuse extensively out of xylem, whereas dissolved ions (e.g. F⁻) may exhibit more restricted flow distributions.¹⁰¹ Despite these differences between the 2 nuclides, both have generally been accepted as tracers for water movement and the use of tracer will depend on the specific objective and process of interest.

Water Dynamics in Plants Subjected to Physical and Chemical Treatments

Given the spatial relationships that can be monitored with positron imaging, scientists have studied localized and long-range plant responses to chemically and physically induced treatments. Specifically, researchers have studied physical disturbances on plants and subsequent impacts on water movement. For example, Kume et al. used an [¹⁸F]F⁻ tracer to monitor

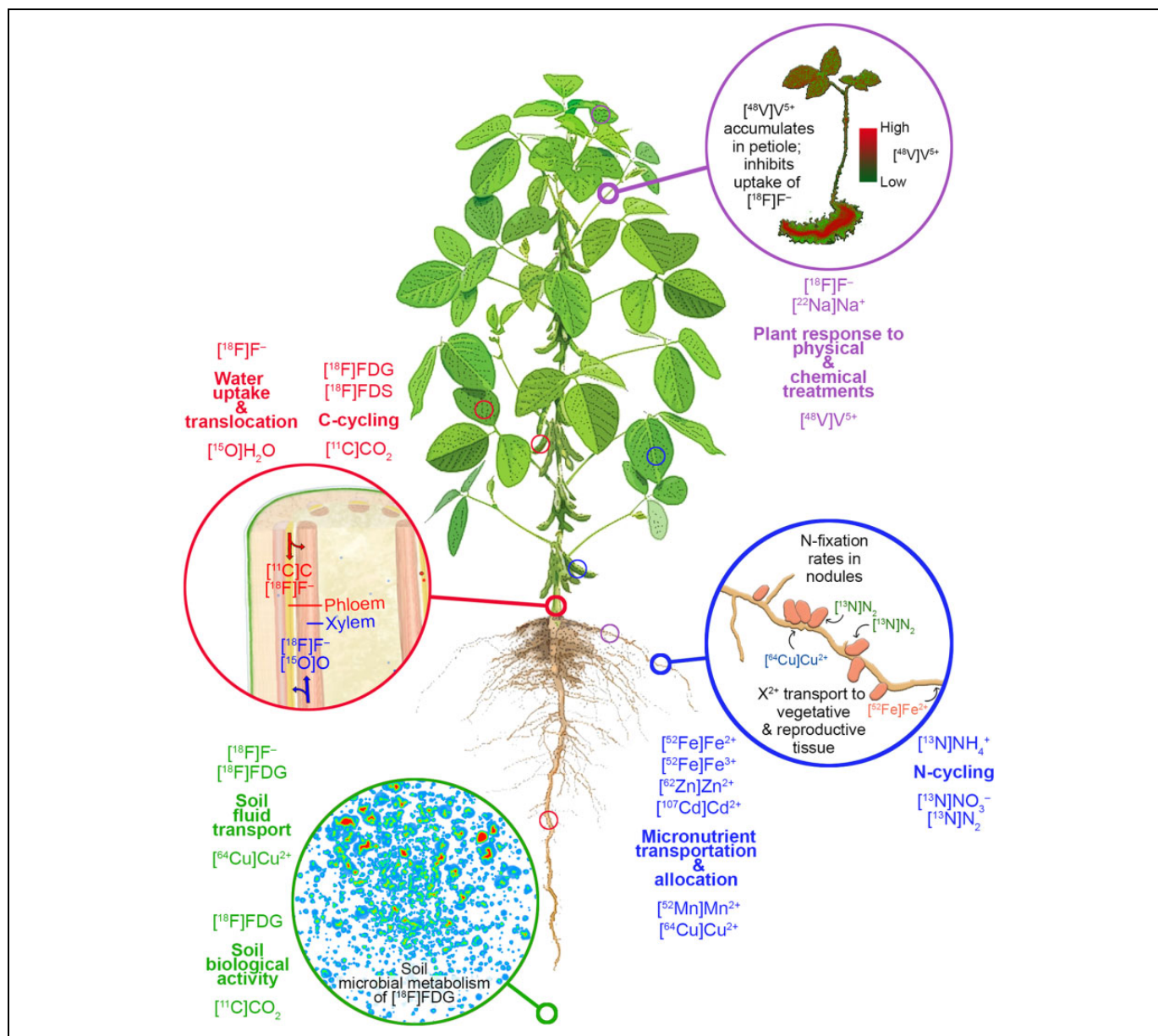


Figure 2. An overview of positron imaging in plants. Examples of key areas of research are outlined in the inserts (thick circles = examples provided here, thin circles = additional cited studies) with experimental results summarized in later figures.

water movement across soybean leaves, with leaf damage at the midrib and radiation exposure as perturbation factors for water movement.²⁸ Damaged leaves demonstrated lower water transport to veins and apex relative to undamaged leaves, with the lamina showing comparable activity. Irradiation of the soybean slowed the uptake of water and resulted in lower tracer uptake over the 30 min duration of the experiment.²⁴ This study implemented a scintillator array to provide real-time imaging of positron distribution in 2-dimensions (PETIS), as opposed to PET which provides a 3-dimensional distribution.

Positron imaging has also been used to evaluate plant responses to chemical treatments, on the local- and whole-plant scales. For example, Furukawa et al. probed the influence

of vanadium, an environmental pollutant which accumulates in plant roots and inhibits plant growth, on water uptake and translocation behavior of a cowpea (*Vigna unguiculata*) plant.²⁵ Using PETIS, they showed water uptake was reduced after the plants had a 20-h pre-treatment with sodium vanadate. The distribution of ⁴⁸V was also imaged across a set of trifoliate cowpea leaves, showing accumulation in the petiole.

In another study on plant response to chemical treatments, Nakanishi et al. used radiographic imaging of [¹⁵O]H₂O to visualize water uptake into the lower part of a soybean stem.³⁰ After applying Al³⁺, water uptake was notably reduced. They also used X-ray film and neutron imaging to resolve fine root structure and water contents. Similarly, Kiyomiya et al.

Table 2. Isotopes Used in Plant Studies, With Associated Half-Lives and Forms Used.

Isotope	Half-life	Form(s) used in plant imaging studies
^{11}C	20.4 m	$[^{11}\text{C}]\text{CO}_2$, ^{15, 22,23,53-80} $[^{11}\text{C}]\text{glutamine}$, ⁷³ $[^{11}\text{C}]\text{indole}$, ⁷³ $[^{11}\text{C}]\text{indole-3-acetic acid}$, ⁷³ $[^{11}\text{C}]\text{indole-3-acetonitrile}$, ⁷³ $[^{11}\text{C}]\text{indole-3-acetamide}$, ⁷³ $[^{11}\text{C}]\text{methionine}$, ^{36,45} $[^{11}\text{C}]\text{methyl jasmonate}$ ⁷⁸
^{13}N	9.97 m	$[^{13}\text{N}]\text{N}_2$, ^{38,41,47,51} $[^{13}\text{N}]\text{NO}_3^-$, ^{20,24,37,41,43,44,46,48} $[^{13}\text{N}]\text{NH}_4^+$, ⁴²
^{15}O	122.2 s	$[^{15}\text{O}]\text{H}_2\text{O}$ ^{27,29,30,32-35}
^{18}F	109.8 m	$[^{18}\text{F}]\text{F}^-$, ^{2,25,26,28,31,32} $[^{18}\text{F}]\text{FDG}$, ^{21,81,82,84-86} $[^{18}\text{F}]\text{fluorodeoxysucrose}$ ($[^{18}\text{F}]\text{FDS}$), ^{83,87} $[^{18}\text{F}]\text{phenylboronic acid}$ ⁹⁷
^{22}Na	2.605 y	$[^{22}\text{Na}]\text{Na}^+$ ⁹⁴
^{48}V	15.98 d	$[^{48}\text{V}]\text{VO}_4^{3-}$, ^{25, 95}
^{52}Mn	5.59 d	$[^{52}\text{Mn}]\text{Mn}^{2+}$, ⁵⁰
^{52}Fe	8.28 h	$[^{52}\text{Fe}]\text{Fe}^{2+}$, ⁴⁰ $[^{52}\text{Fe}]\text{Fe}^{3+}$ -deoxymugineic acid, ^{40,51} $[^{52}\text{Fe}]\text{Fe}^{3+}$ -ethylenediaminetetraacetic acid (EDTA) ³⁹
^{62}Zn	9.22 h	$[^{62}\text{Zn}]\text{Zn}^{2+}$, ⁹³ $[^{62}\text{Zn}]\text{Zn}^{2+}$ -deoxymugineic acid ⁴⁹
^{64}Cu	12.7 h	$[^{64}\text{Cu}]\text{Cu}^{2+}$, ⁵² $[^{64}\text{Cu}]\text{CuO}$ ⁸⁸
^{107}Cd	6.52 h	$[^{107}\text{Cd}]\text{Cd}^{2+}$, ^{89-92,93,96}

Parentheses are not used to denote references here.

investigated water uptake and translocation in a rice plant (*Oryza sativa*) using PETIS imaging with tracer $[^{15}\text{O}]\text{H}_2\text{O}$, and found that adding 80 mM NaCl or 1 mM methylmercury inhibited water uptake at rice roots.²⁷ They also applied biochemical inhibitors to the growth culture solution and observed that these inhibitors reduced translocation from the root system to elsewhere in the rice plant. They proposed that the transport of the inhibitors to leaves resulted in subsequent closure of leaf stomata. Finally, Tsukamoto et al. used PETIS and $[^{15}\text{O}]\text{H}_2\text{O}$ to monitor the effects of treating rice with ALA, used in the biosynthesis of chlorophyll and other biochemical moieties, on water uptake and translocation (Figure 3B).³⁵ They found that generally, ALA treatment increased water translocation rate relative to control plants by 126%, 137%, and 140% at 1.5, 2.5, and 3.5 hours after application. The enhanced rates were reversed with application of ABA, which controls stomatal closure, confirming the proposed mechanism of ALA transport to guard cells.

Water Dynamics in Plants Subjected to Altered Environmental Factors

Water uptake and translocation in plants are sensitive to a variety of environmental factors, including pH of growth medium, light characteristics, and drought conditions. To investigate how these factors influence on the whole-plant scale, researchers used positron imaging to better understand plant partitioning of water under these stressors. An early study of the impact of environmental factors on water uptake by tomato (*Lycopersicon esculentum*) and rice was conducted by Mori et al., who explored how different lighting regimes influenced water uptake and translocation (Figure 3B).²⁹ A similar experiment probing water uptake reflecting light-dark cycling was reported in another study of rice plants.²⁷

Light influence on water uptake in soybean was also investigated, using autoradiography and a BGO scintillator to visualize $[^{15}\text{O}]\text{H}_2\text{O}$.³⁴ As with the PETIS study, this study also demonstrated heavily suppressed water uptake in the dark. Furthermore, the researchers imaged the uptake of water by

soybean under different relative humidities, showing that soybean took up less water at high (100%) humidity relative to lower (50%) humidity, even under optimum lighting.

Nakanishi et al. used PETIS to study water uptake and translocation in common bean and cowpea under water-stressed and sufficient conditions (Figure 3C).³¹ By monitoring activity of $[^{18}\text{F}]\text{F}^-$ in the stem and leaves of both plants, they observed that cowpea maintained water uptake after a drying treatment, unlike common bean. Neutron radiographic imaging of the cowpea plants suggested that water stored in the leaf internode serves as an important source of water for cowpea under simulated drought conditions. In addition to lighting- and moisture-related variables, Kang et al. manipulated growth medium acidity to probe the influence of pH on water uptake and translocation by several rice varieties with different sensitivities to acidity.²⁶ Using $[^{18}\text{F}]\text{F}^-$ as a tracer, PETIS imaging visualized faster and more extensive uptake of water by acid-tolerant rice varieties under the experimental low pH treatment (pH = 3.8) relative to intolerant varieties.

Positron Imaging of Nutrient Dynamics in Plants

Tracers Used for Imaging Nutrient Behavior in Plants

Between plant macronutrients and micronutrients, plant nutrition encompasses a wide range of elements varying in behavior and accessibility to plants. Several of these critical nutrients contain elements that have corresponding positron emitting nuclides, this includes 3 different chemical forms of ^{13}N ($[^{13}\text{N}]\text{N}_2$, $[^{13}\text{N}]\text{NH}_4^+$, and $[^{13}\text{N}]\text{NO}_3^-$) as well as positron-emitting nuclides of essential micronutrients, namely ^{52}Fe , ^{52}Mn , ^{62}Zn , and ^{64}Cu (Table 2). Fe and Zn nuclides were further tailored for use in plant studies through complexation with the siderophore deoxymugineic acid (see Table 2 for references). Additionally, $[^{11}\text{C}]\text{methionine}$ has been used in studies of barley to image nutrient dynamics, not as a nutrient itself, but as a retrieval molecule for Fe. Through these labels, researchers probed fixation, uptake, and translocation of these critical elements using positron-imaging approaches,

Table 3. Summary of Positron Imaging Studies Focused on Plants.

Area of study	Focus of study	Nuclide imaging modality	Reference(s)
<u>Water dynamics in plants</u>			
<i>Water dynamics in plants subjected to physical treatments</i>	Influence of physical disturbance on water movement in soybean leaves	PETIS	28
	Radiation exposure impact on water movement in soybean leaves	PETIS	28
<i>Water dynamics in plants subjected to chemical treatments</i>	Effect of vanadium exposure on water uptake and translocation in cowpea	PETIS	25
	Al application influence on water uptake in soybean stem	Autoradiography	28
	NaCl, methylmercury and other growth inhibitor hindrance of water uptake and subsequent translocation by rice	PETIS	27
<i>Water dynamics in plants subjected to altered environmental factors</i>	5-aminolevulinic acid (ALA) enhancement of water translocation rate in rice	PETIS	35
	Water uptake and translocation by rice and tomato under varying lighting regimes	PETIS	29
	Light-cycling effects on water uptake by rice	PETIS	27
	Influence of differing lighting and relative humidity regimes on water uptake by soybean	Autoradiography and BGO detector system	34
	Uptake and translocation of water by common bean and cowpea under water stress	PETIS	31
	Water uptake and translocation by different varieties of rice under varying light, moisture and pH	PETIS	26
<u>Nutrient dynamics in plants</u>			
<i>Positron imaging of NO_3^- and NH_4^+ dynamics in plants</i>	Uptake and translocation of nitrate in rice	PETIS	37
	Nitrate uptake by soybean and common bean roots under varying nitrogen concentrations	PETIS	44
	Uptake and translocation of nitrate by nodulated and non-nodulated soybean plants	Autoradiography	48
	Uptake and translocation of nitrate by non-nodulated soybean under nitrogen deficient and sufficient conditions	PETIS	46
	Quantification of nitrate uptake and translocation at different sites in kohlrabi plant. Uptake inhibition by methionine sulfoximine was also probed.	PET	43
	Interception of nitrate from red clover by parasitic broomrape	PETIS	98
	Nitrate uptake and translocation by poplar sapling under nitrogen deprivation	PET	24
	Influence of nitrogen deficiency, chemical inhibitors and lighting treatments on ammonium uptake and translocation in rice	PETIS and autoradiography	42
	N_2 fixation by root nodules on soybean	PETIS, ⁹⁹ autoradiography ⁴¹ and PETIS ³⁸	38, 41, 99
	N_2 fixation by grass inoculated with nitrogen fixing bacteria	Autoradiography	47
<i>Positron imaging of micronutrient tracers in plants</i>	Uptake and translocation of Fe^{3+} -deoxymugineic complexes and Fe^{2+} by rice in Fe-sufficient and deficient conditions	PETIS and autoradiography	40
	Influence of Fe-deficiency on uptake and translocation of Fe^{3+} -EDTA complexes by transgenic and control rice plants	PETIS and autoradiography	39
	Uptake and translocation of Fe^{3+} -deoxymugineic acid complexes by barley under Fe-deficient and sufficient growth conditions	PETIS and autoradiography	51
	Translocation of foliage-applied methionine siderophore in barley grown under Fe-deficient and sufficient conditions	PETIS and autoradiography	45
	Fe and S deficiency, aminotransferase inhibitor and methionine pre-treatment effects on translocation of methionine siderophore in barley	PETIS and autoradiography	36
	Mn uptake and translocation by barley under Mn-deficient, Mn-sufficient and Mn-excessive conditions	PETIS and autoradiography	50
	Translocation of Zn^{2+} and Zn^{2+} -deoxymugineic complexes in Zn-deficient and Zn-sufficient rice	PETIS and autoradiography	49
	Uptake and translocation of Cu in soybean	PETIS	52

(continued)

Table 3. (continued)

Area of study	Focus of study	Nuclide imaging modality	Reference(s)
<u>Positron imaging for visualization of carbon dynamics in plants</u>			
Positron imaging for visualization of aboveground photoassimilation processes	Quantification of photoassimilate transport through stem of broad bean	PETIS	71
	Mapping of photoassimilate export rates across a hemp leaf	PETIS	66
	Photoassimilation and sucrose export across a tobacco leaf	PETIS	63
	Comparison of methyl jasmonate and photoassimilate transport in tobacco leaf	Autoradiography	78
	Leaf-scale study of phloem loading mechanisms in aspen, umbrella tree, tali, potato and tomato	Autoradiography	15
	Photoassimilate translocation to wheat ear under varying lighting conditions	PETIS and autoradiography	72
	Photoassimilate translocation into tomato fruits	PET	64
	Photoassimilate translocation to tomato fruits under ambient and elevated CO ₂ levels	PETIS	80
	Fixation of CO ₂ and translocation of photoassimilates in eggplant	PETIS and autoradiography	68
	Distribution of photoassimilates translocated to strawberry fruits	PET, ⁶⁹ PETIS ⁵⁹	59, 69
	Effect of salinity stress on allocation of photoassimilates in tomato plant	PETIS	77
	Phloem transport of photoassimilates in aspen leaves under control and water stressed conditions as well as ambient and elevated CO ₂	PET	60
	Phloem transport of photoassimilates in girdled and ungirdled oak stems	PET	56
	Xylem mediated transport of CO ₂ in poplar leaves under restricted photosynthesis and transpiration	PET and autoradiography	61
	Photoassimilate fate in <i>Arabidopsis</i> under simulated herbivory	Autoradiography	57
Positron imaging used to link above- and belowground photoassimilates	Photoassimilate transport to belowground structures of maize, radish and sugar beet	PET	22
	Determination of maize root growth rates	PET	23
	Photoassimilate partitioning in root system of wild type and mutant maize plants	PET	79
	Photosynthate dynamics throughout a soybean plant	PETIS	66
	Photosynthate dynamics throughout soybean, maize and cucumber plants	PET	79
	Uptake and distribution of photoassimilates in young maize	PET	70
	CO ₂ fixation and metabolism in a fixed photoperiod in wild type and mutant <i>Arabidopsis thaliana</i> seedlings	Autoradiography	76
	Photoassimilate translocation in sorghum	PET	62, 73
	Photoassimilate dynamics in fodder radish	PET	58
	Influence of chemically simulated herbivory on photoassimilate dynamics in aspen	Autoradiography	54
	Gypsy moth herbivory effect on photosynthate partitioning in black poplar	Autoradiography	55
	Western corn rootworm root herbivory impact on whole plant photoassimilate partitioning in maize	Autoradiography	75
	Western corn rootworm root herbivory impact on photoassimilate transformation in maize	PET	74
	Auxin treatment influence on fixation and translocation of photoassimilates	PET and autoradiography	53
Positron imaging used to trace radiolabelled sugars in plants	Translocation of leaf applied [¹⁸ F]FDG in sorghum	Planar BGO detector system and autoradiography	82
	[¹⁸ F]FDG uptake and transport within giant reed seedlings dosed through intact roots, damaged roots, cut stem and cut leaf	PET	85
	[¹⁸ F]FDG uptake into tobacco leaf with varying solution glucose concentrations	PET	86
	Transport of [¹⁸ F]FDG in tobacco leaf	PET	84
	Intercellular exchange of [¹⁸ F]FDG and photoassimilates in tobacco leaf treated with cellulose synthesis inhibitors	Autoradiography	81
	Application of 1' and 6' ¹⁸ F-substituted sucrose analogues in wild type and mutant maize leaves	Autoradiography	87
	[¹⁸ F]FDS transport in wild type and mutant maize leaves	Autoradiography	83
	Influence of wounding and methyl jasmonate treatment on [¹⁸ F]FDG allocation and metabolism in <i>Arabidopsis</i>	Autoradiography	20

(continued)

Table 3. (continued)

Area of study	Focus of study	Nuclide imaging modality	Reference(s)
<u>Positron imaging for visualization of contaminant dynamics in plants</u>			
<i>Positron imaging for visualization of plant uptake and translocation of phytotoxic metals</i>	V uptake and translocation in cowpea	PETIS and Autoradiography	25
	Effect of irradiated chitosan on uptake and translocation of V in rice	Autoradiography	95
	Effect of irradiated chitosan on uptake and translocation of Zn in barley	PETIS	100
	Zn accumulation in <i>Arabidopsis</i> silique, flower, cauline leaf, rosette leaf, and internode	Real time radioisotope imaging system	94
	Uptake and translocation of 10 and 20 nm CuO nanoparticles by lettuce seedlings	PET and autoradiography	88
	Uptake and translocation of Cd by rice at different growth medium Cd concentrations	PETIS	90
	Cd uptake and translocation by rice cultivars of low and high Cd affinity	PETIS and autoradiography	92
	Interactive influence of Zn and Cd on Cd uptake in rice	PETIS	89
	Impact of glutathione and oxidized glutathione on Cd uptake and translocation in oilseed rape	PETIS	93
	Nitrogen source (NO_3^- versus NH_4^+) influence on Cd uptake and translocation in Cd hyperaccumulator <i>Sedum plumbizincicola</i>	PETIS and autoradiography	91
	Cd uptake and translocation by the hyperaccumulator fern <i>Athyrium yokoscense</i> in basal and nutrient-deficient growth media	PETIS and autoradiography	96

visualizing critical spatial relationships governing plant nutrient dynamics. The following discusses how these tracers were used to image nutrient dynamics in plants on the basis of nutrient studied.

Positron Imaging of NO_3^- and NH_4^+ Dynamics in Plants

Of the imaging studies using ^{13}N -labelled nitrogen species, $^{13}\text{N}\text{NO}_3^-$ has been the most extensively used. In 1997, Hayashi et al. were the first to use PETIS to image uptake and translocation of nitrogen-containing species.³⁷ Using a root-applied $^{13}\text{N}\text{NO}_3^-$ tracer, they visualized the uptake and translocation of NO_3^- in a rice plant. PETIS imaging showed rapid translocation of NO_3^- , with activity observed in the leaf sheath within 8 minutes of root application. A stable $^{15}\text{N}\text{NO}_3^-$ tracer was applied to roots as well to probe the fate of NO_3^- translocated to leaves. Furthermore, the authors determined the chemical composition of added NO_3^- in both xylem and phloem transported fluid. Added NO_3^- was transported largely as NO_3^- in the xylem, whereas phloem tissues transported amino acids formed from added NO_3^- .

After Hayashi et al., Matsunami et al. imaged the uptake of NO_3^- by common bean and soybean roots under high and low $^{13}\text{N}\text{NO}_3^-$ treatments.⁴⁴ In both species, 2 distinct regions of accumulation were observed within roots. One of the observed accumulation areas was morphologically linked with a region commonly associated with root hair elongation and rhizobial infectability. Regional accumulation of NO_3^- , as imaged with PETIS, was suggested as a possible inhibitor of root nodule development in subject plants. In another study, Sato et al. used a radiographic bioanalyzer imaging system to image $^{13}\text{N}\text{NO}_3^-$ uptake and translocation on a whole-plant scale

in non-nodulated and nodulated soybean.⁴⁸ They also used PETIS imaging to locally track NO_3^- accumulation in leaves. They observed that the general distribution of NO_3^- was similar within both non-nodulated and nodulated soybean plants. Imaging suggested that NO_3^- initially taken up by roots was transported to the first trifoliate leaf set rather than primary leaves in both types of soybeans.

Similarly, Ohtake et al. also investigated NO_3^- uptake and translocation in a non-nodulated soybean plant, investigating the influence of N-deficient and sufficient growth conditions on behavior.⁴⁶ PETIS imaging was used to visualize the uptake and translocation of NO_3^- to soybean seed pods. They found that translocation of NO_3^- to seed pods was faster under N-deficient growth, with higher net activity in pods under N-deficient conditions as well. Despite this disparity, the authors noted similar amounts of radioactivity in nodes and stems between nitrogen treatments. This report also implemented $^{15}\text{N}\text{NO}_3^-$ as a tracer for nitrate fate in the soybean plants. The authors concluded that ^{15}N labelling was more appropriate for quantitative analysis, whereas ^{13}N labelling provided greater sensitivity and visualization of uptake and translocation in real-time.

Liang et al. used a commercial PET/CT scanner to image uptake and translocation of $^{13}\text{N}\text{NO}_3^-$ by kohlrabi (*Brassica oleracea*), linking regions of active $^{13}\text{N}\text{NO}_3^-$ uptake collected by PET with detailed structural features acquired by CT.⁴³ Through this combined approach, Liang et al. quantified standardized uptake values for different sites on the kohlrabi plant. They noted a high efficiency transport of labelled NO_3^- through a shell-shaped corm structure, which represents the shortest transport route to leaves and buds (Figure 4A). This

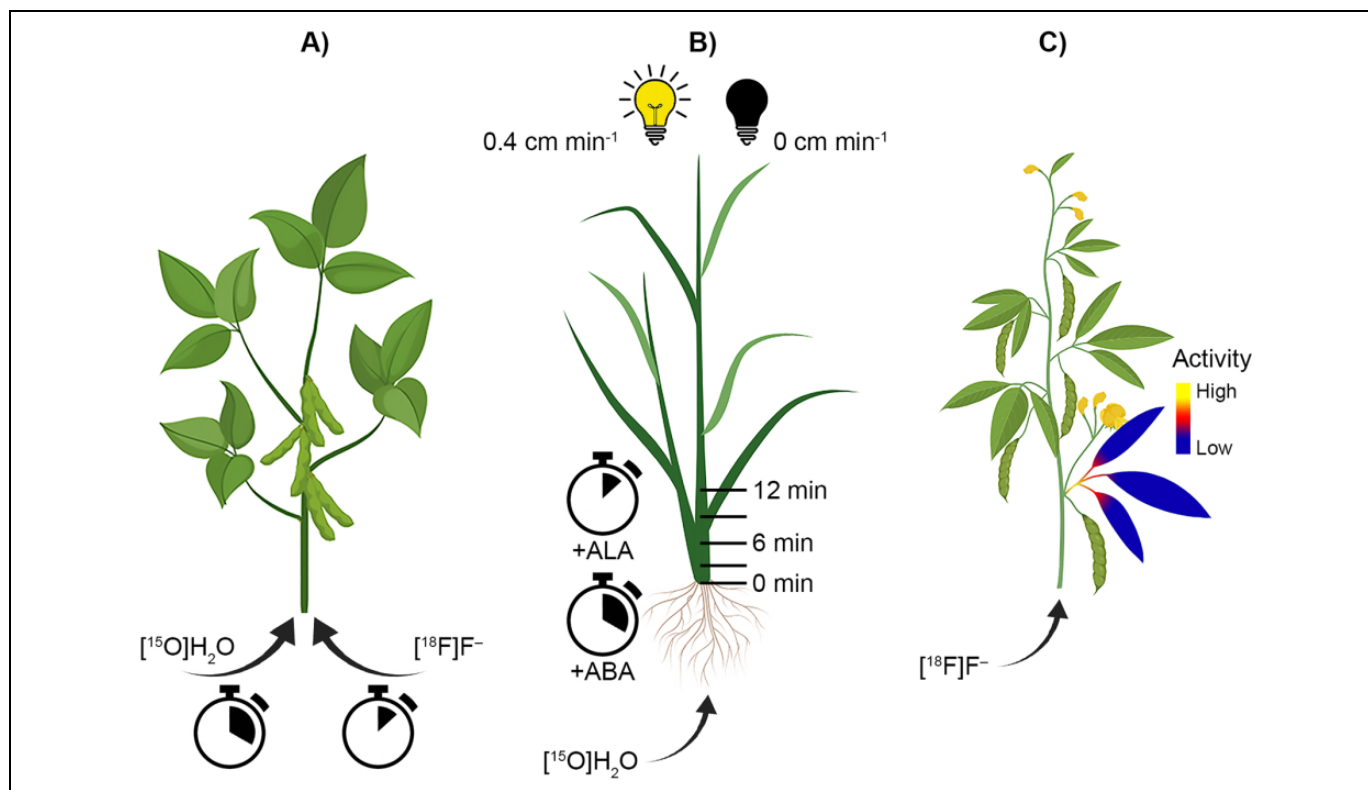


Figure 3. Some examples of positron imaging of plant water dynamics. A) $[^{18}\text{F}]\text{F}^-$ was taken up by soybean more rapidly than $[^{15}\text{O}]\text{H}_2\text{O}$, which suggests $[^{18}\text{F}]\text{F}^-$ may not be a surrogate for water movement tracer in plants.³² However, the low required concentration, low binding to plant tissue, and xylem-mediated flow highlight the utility of $[^{18}\text{F}]\text{F}^-$ as a water tracer over longer time periods. B) Application of ALA, used in chlorophyll biosynthesis, increased water translocation in rice (*Oryza sativa*) by 40% relative to control plants.³⁵ Application of abscisic acid (ABA) reversed the enhanced rates. Horizontal lines indicate the times and positions of the radioactive tracer during the experiment. Light availability affected water translocation differently in rice and tomato plants, increasing rates from 0 to 0.4 cm min⁻¹ and 1.9 cm min⁻¹ and tomato plants under, respectively, 500 $\mu\text{mol m}^{-2} \text{ s}^{-1}$ light intensity.²⁹ Placing plants in darkness following light exposure ceased water uptake. C) Water-stressed and water-sufficient conditions highlight heterospecific differences between cowpea and common bean. Under water-stress, cowpea (*Vigna unguiculata*) maintained water uptake relative to bean, and neutron imaging of $[^{18}\text{F}]\text{F}^-$ indicates water stored in the leaf internode provides moisture during water stress.³¹

study also demonstrated the reversibility of NO_3^- uptake inhibition by methionine sulfoximine.

In addition to probing single plant uptake and translocation, imaging of labelled $[^{13}\text{N}]\text{NO}_3^-$ has been applied as a tracer to study host-parasite interactions.⁹⁸ Kawachi et al. studied NO_3^- dynamics in red clover (*Trifolium pretense*), with and without root-associated parasitic broomrape (*Orobancha* spp.). Using $[^{18}\text{F}]\text{F}^-$ as a conservative tracer for volume normalization, the authors were able to image and quantify $[^{13}\text{N}]\text{NO}_3^-$ interception from red clover by broomrape. Interception was determined to be around 74%, representing a substantial diversion of NO_3^- from the host.

Of the papers surveyed, we found one imaging study that implemented $[^{13}\text{N}]\text{NH}_4^+$ with PETIS and radiographic imaging. This study investigated how nitrogen deficiency, treatment with inhibitors, and lighting treatments influence $[^{13}\text{N}]\text{NH}_4^+$ uptake and translocation in rice.⁴² In the control plant grown under ideal conditions with no inhibitors, uptake into roots was rapid, with subsequent ^{13}N movement from the discrimination center at the base of the rice plant to the newest

leaf. Nitrogen deficiency enhanced translocation of ^{13}N to the discrimination center under low light conditions but reduced accumulation under full light. Full dark conditions resulted in reduced nitrogen uptake but not a complete cessation, despite the shutdown of water flow. Methionine sulfoximine treatment inhibited NH_4^+ uptake and translocation. Treatment with ABA enhanced accumulation in the basal portion of the stem, which served as a point of resource distribution and was identified as the discrimination center by the authors. This treatment inhibited translocation elsewhere in the plant.

Positron Imaging to Investigate N_2 Fixation Processes in Plants

Using $[^{13}\text{N}]\text{N}_2$ and PETIS, Ishii et al. visualized N_2 fixation *in vivo*, providing a novel perspective on this process critical to life on Earth. They first imaged $[^{13}\text{N}]\text{N}_2$ fixation by root nodules on a set of soybean plants.³⁸ Using PETIS imaging, they observed localized zones of $[^{13}\text{N}]\text{N}_2$ fixation in real-time. Using activity measurements from PETIS, they estimated the

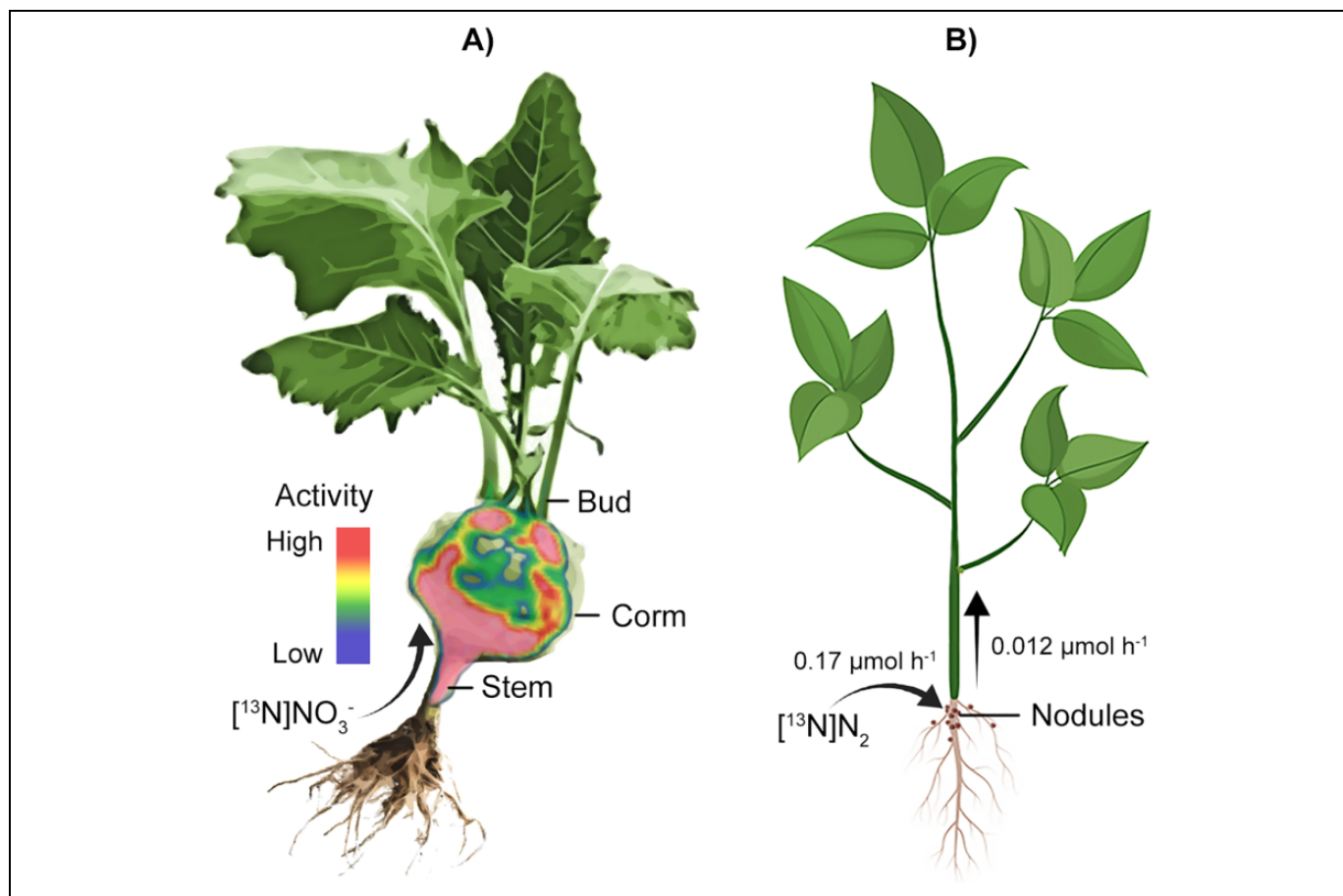


Figure 4. Examples of positron imaging of plant nitrogen dynamics. A) Using a combination of positron emission tomography (PET) and computerized tomography (CT) scanning, Liang et al.⁴³ identified and quantified uptake and translocation of $[^{13}\text{N}]\text{NO}_3^-$ through kohlrabi. The most efficient transport of $[^{13}\text{N}]\text{NO}_3^-$ was through the corm, which represented the shortest transport to leaves and buds. B) PETIS imaging of $[^{13}\text{N}]\text{N}_2$ was used to quantify nitrogen fixation and export from Rhizobia nodules on soybean roots.³⁸ The PET image in A) was adapted with permission from (Liang et al.⁴³). Copyright (2011) American Chemical Society.

N_2 fixation rates for nodules on 6 soybean plants to be $0.17 \mu\text{mol N}_2 \text{ h}^{-1}$ (Figure 4B). Also, from the PETIS measurements, they were able to determine the decreasing rate, or the rate of nitrogen export from nodules. They calculated an export rate of $0.012 \mu\text{mol N}_2 \text{ h}^{-1}$. This demonstrates the power of positron imaging for estimating fixation and transport rates. Kasel et al. applied $[^{13}\text{N}]\text{N}_2$ to a soybean plant.⁴¹ $[^{13}\text{N}]\text{N}_2$ fixation by roots was visualized by autoradiographic imaging. More recently, Yin et al. incubated a soybean plant with $[^{13}\text{N}]\text{N}_2$ and then imaged its root system using PET, effectively imaging regions where N_2 fixation occurred.

One study has been reported on radiographic imaging of N_2 fixation by *Setaria viridis*, a model grass species, inoculated with nitrogen fixing bacteria (*Herbaspirillum seropedicae* and *Azospirillum brasilense*).⁴⁷ This work demonstrated fixation of $[^{13}\text{N}]\text{N}_2$ by inoculated plant roots with autoradiography and thin-layer chromatographic (TLC) analysis of biochemical extractions, which traced fixed ^{13}N into ribulose-1,5-bisphosphate carboxylate. N_2 fixation was further highlighted by relative decay analysis on plant tissues, which were exposed to traces of $[^{11}\text{C}]\text{CO}_2$ during $[^{13}\text{N}]\text{N}_2$ dosing. Inoculated plant

tissue, which was cut to prevent further tracer movement, showed decay characteristics representative of ^{13}N and ^{11}C uptake as opposed to uninoculated plants, which showed decay characteristics of ^{11}C only. This suggested that uninoculated plant tissues contained no fixed ^{13}N and just traces of fixed $[^{11}\text{C}]\text{CO}_2$. This study also utilized $[^{11}\text{C}]\text{CO}_2$ dosing to test whole plant carbon metabolism of inoculated and uninoculated nitrogen-limited plants. Inoculated plants did not show the same disturbances in carbon dynamics as uninoculated nitrogen-limited plants (i.e., a reduction in $[^{11}\text{C}]\text{CO}_2$ fixation, increase in $[^{11}\text{C}]\text{photoassimilate}$ transport from leaves to roots, decrease in $[^{11}\text{C}]\text{sugar}$, and increase in $[^{11}\text{C}]\text{amino acid}$ partitioning).

Positron Imaging of Micronutrient Tracers in Plants

Because Fe represents an essential plant micronutrient with limited availability in many environmental systems, plant Fe acquisition and allocation processes are of great interest. Due to the spatial aspects of these critical processes and the availability of a suitable positron-emitting tracer (^{52}Fe), Fe dynamics in plants have been the focus of positron imaging studies. For

example, Ishimaru et al. used PETIS and a radiographic bio-imaging analyzer system to explore the role of Fe chemistry on the uptake and translocation of Fe in rice grown under Fe-sufficient and -deficient conditions.⁴⁰ This work served as a visual demonstration that in addition to taking up Fe^{3+} complexed with the siderophore deoxymugineic acid, free Fe^{2+} could be taken up by rice through a previously unobserved pathway. PCR analyses indicated the OsIRT1 protein likely played an important role in rice uptake of Fe^{2+} .

A later study also used PETIS and radiographic imaging to probe the uptake and translocation of Fe by transgenic rice.³⁹ They found that rice modified with the *ref1/372* chelate-reductase gene took up more $^{52}\text{Fe}]\text{Fe}^{3+}\text{-EDTA}$ than its control counterpart under Fe-deficient conditions (Figure 5A). Additionally, the distribution of Fe in the modified plant was different than in the control, with greater accumulation observed in the stem and leaf in transformed rice compared to the vector control.

Using PETIS and a radiographic bio-imaging analyzer system, Tsukamoto et al. probed the uptake and translocation of Fe in barley grown under Fe-deficient and Fe-sufficient conditions and under light and dark conditions.⁵¹ For all conditions studied, $^{52}\text{Fe}]\text{Fe}^{3+}\text{-deoxymugineic acid}$ complexes were translocated to the discrimination center at the basal region of the stem before redistribution elsewhere. Deficient barley showed greater uptake and subsequent translocation to shoots than sufficient barley. In conditions with no light, translocation was shifted more toward younger leaves than older leaves.

Use of positron imaging with $^{11}\text{C}]\text{methionine}$ as a siderophore precursor to investigate Fe acquisition in barley plants has been reported as well.^{36,45} In one of these studies, foliar application of methionine to Fe-deficient barley resulted in translocation of methionine from the applied leaf to the discrimination center, followed by translocation to leaves exhibiting chlorosis (Figure 5B).⁴⁵ In Fe-sufficient barley, applied methionine was also translocated to the discrimination center at the base of the stem, but was then moved to new leaves in the absence of chlorotic leaves. In the other study, when $^{11}\text{C}]\text{methionine}$ was applied to barley roots grown under Fe-deficient and S-deficient conditions, in the presence of an aminotransferase inhibitor and with methionine pretreatment, the discrimination center also played an important role in methionine distribution in all treatments.³⁶ Fe-deficiency reduced methionine translocation to shoots from the discrimination center, while Fe-sufficient and pretreated barley translocated relatively more methionine to shoots. Application of an aminotransferase inhibitor enhanced translocation to shoots. S-deficiency reduced methionine translocation to shoots from roots, including the discrimination center.

In addition to these studies focusing on Fe, Mn uptake and translocation in barley under Mn-deficient, -sufficient, and -excessive conditions were imaged.⁵⁰ In all treatments, $^{52}\text{Mn}]\text{Mn}^{2+}$ taken up by roots accumulated first in the discrimination center. Mn-deficient barley relocated more Mn to young shoots from the discrimination center compared to barley grown under Mn-sufficient and Mn-excessive conditions (Figure 5C). The importance of the discrimination center was

highlighted further when Mn was applied to the leaf of an Mn-sufficient plant, after which Mn was traced to the discrimination center and accumulated within 27 minutes.

Similar imaging studies have been carried out using positron-emitting Zn tracers. Suzuki et al. probed the influence of deoxymugineic acid complexation with $^{62}\text{Zn}]\text{Zn}^{2+}$ on translocation in rice.⁴⁹ Radiographic and PETIS imaging of Zn-deficient plants showed that deoxymugineic acid complexation enhanced the long-distance transport of Zn in both root- and leaf-applied treatments.

In addition to Fe, Mn, and Zn, Cu has also been studied for its usefulness as a tracer in plant research as positron-emitting ^{64}Cu .⁵² The authors used PETIS to demonstrate the efficacy of ^{64}Cu , produced by the $^{64}\text{Ni}(\text{p}, \text{n})^{64}\text{Cu}$ reaction with a ^{64}ZnO target, as a probe for imaging soybean tissues.⁵² Specifically, over 72 h of imaging, they demonstrated soybean uptake of the ^{64}Cu tracer from the root to leaves. Preferential accumulation of ^{64}Cu was observed in the nodes, but ^{64}Cu was observed in the stem and young leaves as well.

Positron Imaging for Visualization of Carbon Dynamics in Plants

Tracers Used for Imaging Carbon Partitioning in Plants

The primary positron-emitting tracer used for probing carbon dynamics in plants is gaseous $^{11}\text{C}]\text{CO}_2$. Despite its short half-life of 20.4 minutes, relatively rapid photoassimilation and translocation processes in plants allow fixed $^{11}\text{C}]\text{CO}_2$ to be visualized on a whole-plant scale (i.e., from roots-to-shoots) throughout a wide diversity of plant species. Furthermore, visualization of the spatial partitioning of fixed CO_2 allows for subsequent targeted analyses (e.g., TLC or HPLC) to determine assimilation into specific molecules or classes of molecules.

In addition to photosynthesis, studies imaging the uptake and translocation of specific sugar analogues in plants, rather than an array of photoassimilates, are included here. The primary tracer used to probe sugar translocation is the commonly used $^{18}\text{F}]\text{FDG}$. As a PET labelled form of glucose, this tracer is generally regarded as an analog for glucose in terms of its behavior, but the modes by which it is transported and metabolized in plants are not entirely understood.¹⁰² ^{18}F has also been used to label sucrose ($^{18}\text{F}]\text{FDS}$) at different positions on the glucosyl and fructosyl moieties for application to plant imaging, providing an alternative to $^{18}\text{F}]\text{FDG}$. Studies visualizing incorporated $^{11}\text{C}]\text{CO}_2$ and ^{18}F -labelled sugars in plants as well as others determining the biochemical incorporation into specific molecules are overviewed in the sections below, delineated by context in which photoassimilation is studied.

Positron Imaging for Visualization of Aboveground Photoassimilation Processes

Positron imaging of plant fixation of $^{11}\text{C}]\text{CO}_2$ and translocation within aboveground plant structures has seen widespread application, allowing visualization of fixed carbon

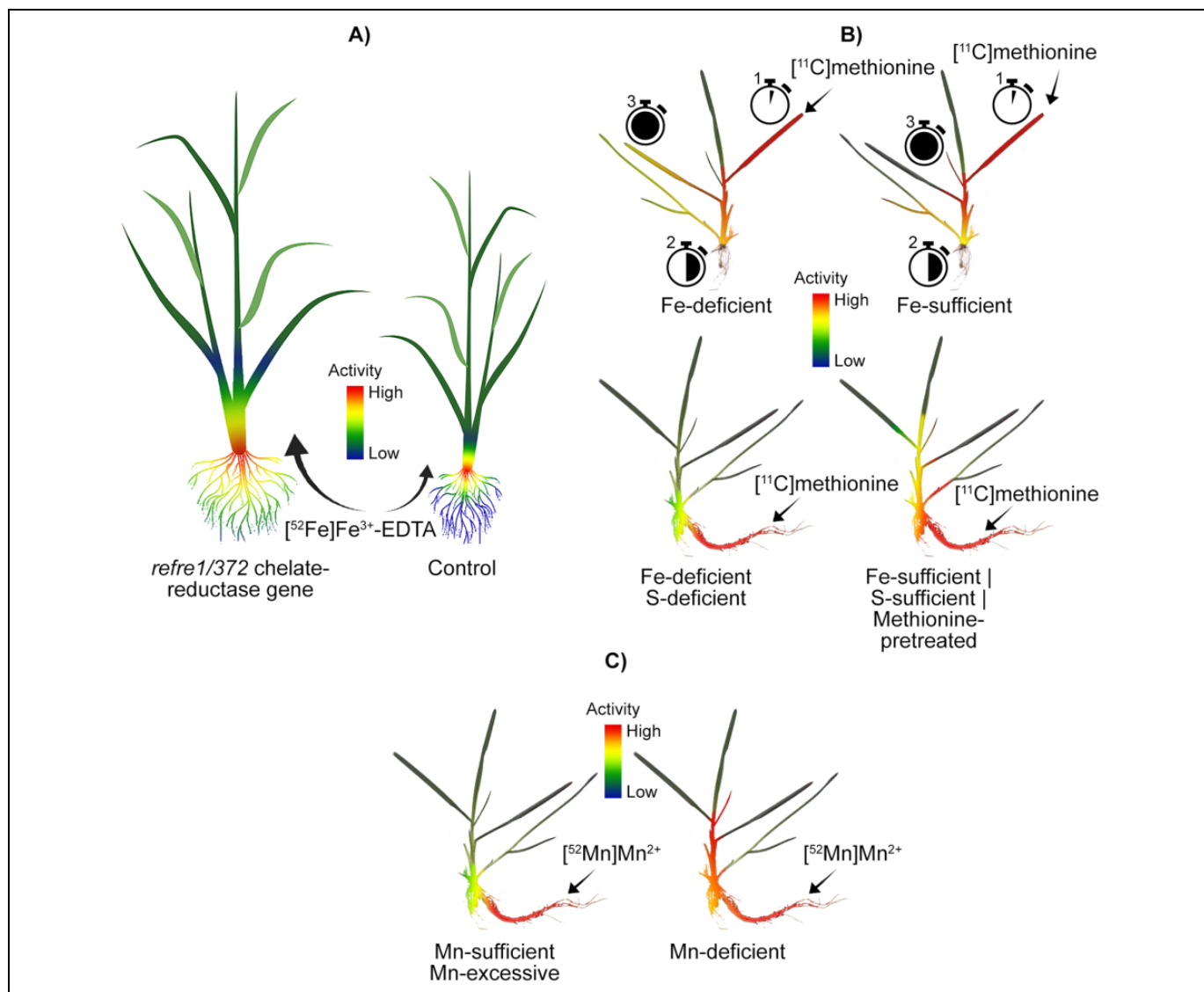


Figure 5. Examples of micronutrient analyses using positron imaging. A) PETIS was used to track uptake and translocation of Fe in transgenic rice. Under Fe-deficient conditions, rice modified with the *refre1/372* chelate-reductase gene took up more $[^{52}\text{Fe}]\text{Fe}^{3+}\text{-EDTA}$ relative to a control, accumulated more Fe in stem and leaves, and grew more vigorously.³⁹ B) PETIS imaging of barley with $[^{11}\text{C}]\text{methionine}$ as a siderophore precursor revealed application at a cut leaf (1) first travelled to the discrimination center (2; intersection between root and shoots), and then to chlorotic foliage (3) under Fe-deficient conditions.⁴⁵ In Fe-sufficient barley, Fe travelled to the discrimination center, but was ultimately sequestered in new foliage in the absence of chlorotic leaves. When $[^{11}\text{C}]\text{methionine}$ was applied to barley roots under deficient (Fe, S) conditions, methionine translocation from the discrimination center was reduced relative to barley grown under Fe/S-sufficient conditions and/or treated with an aminotransferase inhibitor.³⁶ C) Barley grown under Mn-deficient conditions, translocated more root-applied $[^{52}\text{Mn}]\text{Mn}^{2+}$ from the discrimination center to new foliage relative to barley grown under Mn-sufficient/excessive conditions.⁵⁰

translocation to specific structures (e.g., fruits, stems, leaves) and throughout aboveground biomass. This allows for spatially resolving assimilation and export parameters on the local- and whole-plant scale for fine-scale phenotyping. An early use of $[^{11}\text{C}]\text{CO}_2$ as a tracer for photoassimilation was by Matsuhashi et al., who used PETIS to quantify the transport of leaf-fed $[^{11}\text{C}]\text{CO}_2$ through the stem of a broad bean (*Vicia faba*) plant.⁷¹ They used transfer function analysis, which was developed in 1978 to estimate time dependency of parameter values, to successfully model flow speeds and distribution patterns of photo-assimilates, effectively quantifying key photosynthetic

parameters (Figure 6A).¹⁰³ Likewise, Kawachi et al. used an $[^{11}\text{C}]\text{CO}_2$ tracer to image photoassimilation and sucrose export rates across a hemp (*Cannabis sativa*) leaf, using PETIS to quantitatively map physiological parameters on the single-leaf scale.⁶⁶

PETIS imaging was also used to quantify photoassimilation and sucrose export across a tobacco leaf.⁶³ Photoassimilate transport was imaged across tobacco (*Nicotiana tabacum*) leaves and compared with the movement of $[^{11}\text{C}]\text{methyl jasmonate}$, a signaling molecule, using autoradiography.⁷⁸ More extensive transport of methyl jasmonate was observed

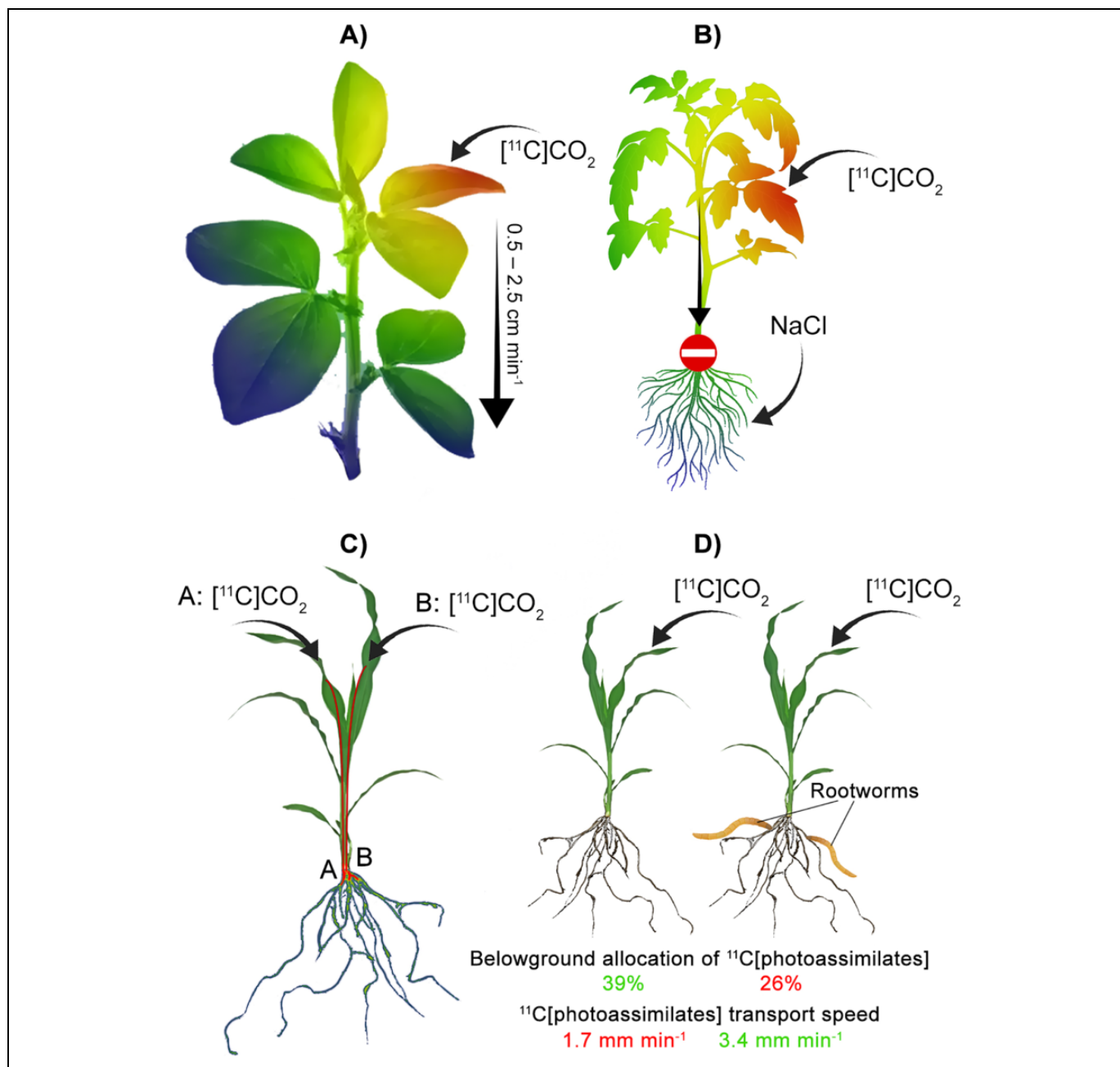


Figure 6. Examples of positron imaging of carbon transportation and allocation dynamics. A) PETIS was used to model phloem transport of ^{11}C photoassimilates within a broad bean plant.⁷¹ Results indicated phloem transport speeds increased in farther internodes from the dosed leaf and were also greater using enriched CO_2 . B) Salinity-induced stress reduced transportation of ^{11}C photoassimilates to the basal stem and roots of a tomato plant, resulting in accumulation in the leaves.⁷⁶ C) A combination of magnetic resonance imaging (MRI) and PET was used to quantify sectorial source-sink photoassimilate partitioning in maize.²² Uptake of ^{11}C by specific leaves was linked with correspondingly specific regions of accumulation in maize roots. D) PET was used in conjunction with amino acid, sugar, and hormone quantification to characterize the effects of rootworm herbivory on maize roots.⁷⁴ Browsed maize plants had increased transport despite reduced allocation of ^{11}C photoassimilates to damaged roots.

compared with that of assimilated ^{11}C CO_2 , which moves by phloem transport. This led the authors to conclude that methyl jasmonate likely moved through xylem and phloem tissues in the leaves studied.

Leaf-scale radiographic imaging studies of aspen (*Populus tremula*), umbrella tree (*Maesopsis eminii*), tali (*Erythrophleum*

suaveolens and *E. ivorens*), tomato, and potato (*Solanum tuberosum*) were conducted to determine leaf phloem loading mechanisms in these species.¹⁵ Using gradients in ^{11}C -photoassimilate density across veins in these leaves, it was determined passive loading (i.e., photoassimilate transport from high to low concentrations) occurred in aspen, tali, and young

umbrella tree leaves. Mature umbrella tree leaves, tomato, and potato followed an active phloem loading strategy (i.e., photoassimilate transport from low to high concentrations). This work demonstrated the applicability of radiography with [^{11}C] photoassimilates to investigate distinct phloem loading strategies in morphologically and physiologically distinct leaves.

Positron imaging was also used to study photoassimilate allocation to seed-bearing fruit and grain structures in plants, providing a novel perspective on the direct link between carbon fixation and specific sinks on these structures. For example, allocation of leaf-fed [^{11}C]CO₂ on an individual wheat (*Triticum aestivum*) ear scale was imaged with PET under 3 different light conditions.⁷² Translocation of photoassimilates was imaged on an individual grain scale, with sequential grain filling and uneven storage of photoassimilates observed. Translocation rates from dosed leaf to the wheat ear decreased with decreasing light treatment from full-light to shade to dark.

Another study used PET imaging to investigate the movement of photoassimilates into tomato fruits.⁶⁴ Photoassimilates were imaged in real-time flowing into small and large tomato fruits from the plant stem. Later, a whole-plant study used PET to image the fixation of CO₂ and translocation to tomato fruits.⁸⁰ This study found that plants grown under elevated CO₂ levels (1500 and 3000 ppm CO₂) showed greater translocation of photoassimilates to fruit relative to plants grown under ambient levels (400 ppm CO₂).

Imaging the fixation of [^{11}C]CO₂ by eggplant (*Solanum melongena*) and translocation through the stem and into fruit was also performed.⁶⁸ Using PETIS imaging of the intact plant and radiographic imaging of sectioned fruit, heterogeneity in photoassimilate distribution across the fruit was observed. Preferential partitioning was linked to vascular system architecture. Similarly, PET was used to image photoassimilate distribution on an individual fruit of a strawberry plant (*Fragaria x ananassa* Duch. cv. Fukuoka S6) plant.⁶⁹ As with the previous study with eggplant, translocation of fixed carbon within strawberry fruits was heterogeneous. Localized accumulation within fruit was proposed to be associated with the specific leaf that fixed the CO₂ to be translocated to the fruit. Another study imaged photoassimilate translocation to strawberry fruits and found a similar link between source leaf and fruit partitioning.⁵⁹ In addition to partitioning heterogeneity within fruits, this study observed selective distribution across imaged fruits. A stable ^{13}C tracer experiment was used to reinforce relative partitioning observed with ^{11}C imaging.

Within the context of aboveground plant processes, positron imaging has been used to monitor responses of photoassimilate dynamics to external disturbances and environmental changes. For example, Suwa et al. studied the influence of salinity-induced stress on the allocation of fixed [^{11}C]CO₂ by a tomato plant (Figure 6B).⁷⁷ Using PET imaging, they found that salinity hindered ^{11}C transport to the basal portion of the stem and roots, leading to photoassimilate accumulation in the leaves. These partitioning trends were reflected with ^{13}C tracing as well. PET imaging and mathematical modeling of phloem transport processes in aspen leaves were performed under

control and water-stressed conditions to probe phloem transport dynamics in plants grown under ambient (404 ppm) and elevated (659 ppm) CO₂ levels.⁶⁰ Compared to plants grown under ambient CO₂ levels, plants grown under elevated CO₂ had leaves with the highest phloem transport speeds when imaged under sufficient water conditions; however, these plants also showed a greater reduction in transport rates when exposed to drought. Another study imaged an oak (*Quercus robur*) tree after disturbance by girdling in order to probe phloem transport of photoassimilates.⁵⁶ Oak responded to stem girdling by increasing the flow within phloem elsewhere, highlighting the resilience of phloem transport. This study used MRI to provide complementary structural details in the oak stem.

Disturbance-induced treatments for the purpose of teasing apart transport mechanisms has been reported on the leaf-scale as well.⁵⁹ Using light limitation and leaf greasing to restrict photosynthesis and transpiration, respectively, xylem-mediated transport of [^{11}C]CO₂ was probed in poplar leaves using a combination of PET and autoradiography. Herbivory was simulated by applying methyl jasmonate to damaged *Arabidopsis* leaves; on the plant-scale, photoassimilate partitioning was imaged by radiography.⁵⁷ ^{11}C applied as CO₂ was traced into methyl jasmonate treated leaves, where photoassimilates were transported from sink tissues. With TLC of plant extracts, ^{11}C translocated to treated leaves was shown to be assimilated into the phenolic compound cinnamic acid.

Positron Imaging Used to Link Belowground Translocation of Photoassimilates

Given the penetrating ability of gamma rays emitted upon positron annihilation, positron imaging is well suited for visualizing processes in opaque materials that may be challenging to probe otherwise. This makes positron imaging uniquely capable of non-invasively detecting and imaging processes in plant rooting systems in soils, providing a bridge between root structure and activity unparalleled by other approaches, particularly when coupled with high resolution imaging techniques like CT and MRI. In combination with aboveground images accessible by whole-plant visualization, positron imaging serves as a powerful tool for tracing photoassimilate dynamics throughout plants. Studies presented here incorporate positron imaging studies of the partitioning of [^{11}C]photoassimilates to root structures in plants, with many incorporating imaging of aboveground structures as well.

A study reported by Jahnke et al. uses a combination of PET and MRI imaging to trace photoassimilated [^{11}C]CO₂ belowground in maize (*Zea mays*), radish (*Raphanus sativus*), and sugar beet (*Beta vulgaris*) plants.²² Combining the high resolution structural images from MRI and regions of active photoassimilate accumulation from PET, the authors observed sectorial source-sink photoassimilate partitioning in sugar beet and radish, with uptake of [^{11}C]CO₂ by specific leaves linked with correspondingly specific regions of accumulation in the belowground biomass. ^{11}C was traced to maize roots, where MRI and PET were used to quantify root growth rates

(Figure 6C). Wang et al. also used PET to determine root growth rates. They used reconstructed PET and OPT images in conjunction to link regions of structural root growth with zones of photoassimilate partitioning.²³ They concluded that PET/OPT is a particularly suitable tool for root phenotyping, as it may serve as a predictor of where new root expansion may occur through active photoassimilate accumulation not visible by other means alone. In another study investigating the root systems of maize, PET was used to compare photoassimilate partitioning in the root systems of young wild type and mutant maize plants.⁷⁹ Images from this study showed a wider distribution of active root growth at meristems in the root system of the mutant maize compared with the wild type.

An example of whole-plant imaging of photoassimilate dynamics in soybean using PETIS demonstrated the distribution of photoassimilates throughout the plant.⁶⁶ Fixed ^{11}C was traced from leaves into stems and then into roots, with an estimated 40% of photoassimilates translocated to the root system within 1 hour. Decay corrected activities of fixed carbon from PETIS within 1 hour showed that the mass of fixed carbon was conserved within the subject plant, suggesting fixed carbon was not used for respiration within the studied time period (1 hour). In another study using PET imaging of whole-plant photoassimilate translocation in soybean, the authors found preferential translocation of fixed ^{11}C toward seed pods.⁷⁹ This study also imaged photoassimilate movement in whole young cucumber (*Cucumis sativus*) and maize plants. Fixed ^{11}C accumulated more in cucumber flowers than in the stem and leaves. Maize showed activity throughout the plant, from the shoots to the root tips, over 119 minutes of imaging. [^{11}C]photoassimilate partitioning in young maize plants was imaged using a PhytoPET imaging system, with uptake and distribution of [^{11}C]photoassimilates imaged throughout the subject plant.⁷⁰

Song et al. used an [^{11}C]CO₂ tracer to probe CO₂ fixation and metabolism across a fixed photoperiod in *Arabidopsis thaliana* seedlings.⁷⁶ Here, they examined performance of mutant lines possessing deficiencies in either starch biosynthesis or its degradation with wild-type to understand how plant starch regulation influences whole-plant physiology and metabolism of carbon resources. Radiographic imaging of seedlings showed relatively higher allocation of photoassimilates to roots by starch synthesis deficient mutants than wild type plants and starch degradation deficient genotypes.

Karve et al. used a commercial PET scanner to image photoassimilate translocation in sorghum (*Sorghum bicolor*) plants grown to vegetative and reproductive stages.⁶² Due to the size of the scanner, which was capable of imaging a human body, whole-plant imaging of mature sorghum was possible. Imaging at the vegetative and reproductive stages revealed no significant differences in transport rates between these growth stages. Transport speeds were highest in the leaf blades, followed by stem and roots. Reproductive stage sorghum fixed less carbon than the vegetative stage plant. Allocation in the reproductive stage sorghum was more heavily weighted toward the apex as compared to vegetative plants, which showed greater allocation to lower stem and roots. This work underscores the importance

of simultaneously accessing multiple regions of interest to assess speeds, which is made possible by PET imaging, as speeds may vary greatly across an individual plant.

Mudgil et al. observed similar results when they imaged [^{11}C]CO₂ fixation and translocation in sorghum. They found that sorghum at the grain-filling stage accumulated throughout the stem and the grain head.⁷³ Movement of fixed carbon to roots also occurred rapidly. In another study, Garbout et al. used whole-plant PET imaging to study photoassimilate dynamics in fodder radish.⁵⁸ PET showed distribution of ^{11}C throughout the radish plant but accumulated mostly in the main root. They also used CT to produce detailed images of the radish root structure and the sand matrix in which the plant was growing. Thus, this study shows the potential application of PET/CT to the non-invasive study of plant-soil interfaces.

The response of root partitioning photoassimilate to chemical treatments and chemical/physical disturbances has been studied as well. For example, the influence of jasmonic acid treatment, as a form of simulated herbivory, on whole-plant photoassimilate dynamics in aspen was imaged.⁵⁴ Compared to untreated plants, plants treated with jasmonic acid shifted translocation of fixed [^{11}C]CO₂ away from leaves, with the roots and stem more readily receiving photoassimilate exports. Accompanying biochemical analysis of leaves from treated and untreated plants showed export of starch from leaves was enhanced by jasmonic acid treatment.

Radiography was also used to image the influence of gypsy moth leaf herbivory on photoassimilate partitioning on black poplar (*Populus nigra*).⁵⁵ Similar to the previous study that used a chemical analog for herbivory, this study found enhanced export of recently fixed photoassimilates from the attacked leaves. Additionally, more herbivory-stimulated accumulation of photoassimilate was noted in the base (i.e., away from roots and young shoots) relative to control plants. Another study used an [^{11}C]CO₂ tracer to investigate Western corn rootworm herbivory of maize roots and its influence on whole-plant photoassimilate partitioning.⁷⁵ Radiographic imaging of control and infested roots showed lower translocation of recently fixed ^{11}C to root tips. Activity was also traced into rootworm larvae using this approach. The enhanced allocation of photoassimilates to leaves and stems in infested maize plants accompanied this change to root activity. Finally, rootworm herbivory on maize roots was investigated in a later study, where PET was used in conjunction with amino acid, sugar, and hormone quantification to develop a detailed perspective on herbivory and related hormone dynamics.⁷⁴ Browsed plants had reduced belowground partitioning of [^{11}C]photoassimilates in attacked roots (Figure 6D). Root herbivory stimulated a change in locally regulated root auxin synthesis from indole-3-pyruvic acid to indole-3-acetonitrile. Root herbivory also enhanced the export of newly synthesized amino acids to roots. It should be noted that this study made use of a suite of ^{11}C -labelled auxins (Table 2) to trace hormone movement.

The interplay between auxins and belowground partitioning of photoassimilates was also investigated by Agtuca et al., who studied the influence of root application of indoleacetic acid

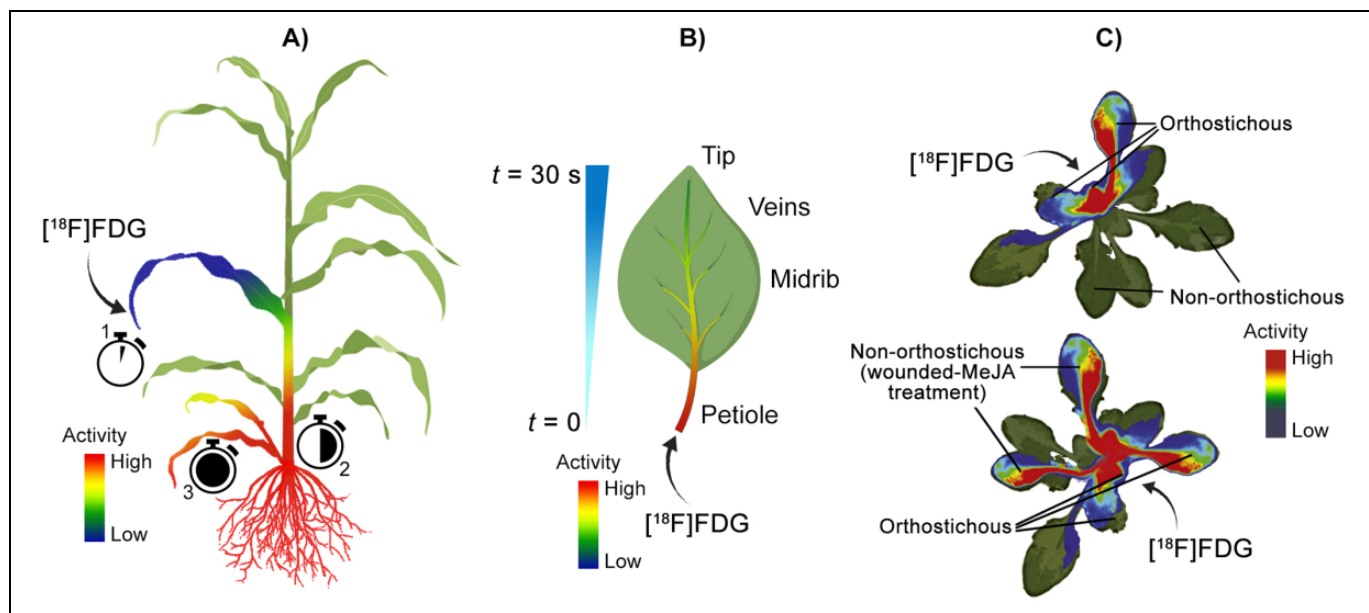


Figure 7. Examples using positron imaging to trace radiolabelled sugars in plants. A) First use of $[^{18}\text{F}]\text{FDG}$ imaging in plants.⁸² $[^{18}\text{F}]\text{FDG}$ was applied through the leaf of a sorghum plant, which was first translocated to the discrimination center at the base of the shoots, followed by redistribution to roots and young leaves. B) Intra-leaf transportation of $[^{18}\text{F}]\text{FDG}$ in tobacco plants.⁸⁴ The leaf petiole and midrib dominated the initial $[^{18}\text{F}]\text{FDG}$ uptake, followed by slower distribution into smaller veins determined by physicochemical properties; however, radioactivity was detected at the leaf tip within 30 seconds of $[^{18}\text{F}]\text{FDG}$ application. C) $[^{18}\text{F}]\text{FDG}$ allocation and metabolism in wounded and methyl-jasmonate-treated rockress (*Arabidopsis*).²¹ $[^{18}\text{F}]\text{FDG}$ applied to a cut petiole in rockress was transported to orthostichous (arranged vertically) leaves in control plants, though diverted to wounded and methyl jasmonate-treated (MeJA) leaves in treated plants. The PET imagery in C) was adapted from *Nuclear Medicine and Biology*, 39(8), Ferrieri AP, Appel H, Ferrieri RA, & Schultz JC. Novel application of 2- $[^{18}\text{F}]\text{fluoro-2-deoxy-D-glucose}$ to study plant defenses, 1152-1160, Copyright (2012), with permission from Elsevier.

and salicylic acid on photosynthetic fixation of CO_2 and translocation of photoassimilates.⁵³ PET and radiographic imaging visualized the reduction of photoassimilate export, below-ground allocation, and transport of photoassimilates in roots caused by indoleacetic acid application. Salicylic acid, on the other hand, increased leaf export of ^{11}C as well as transport speeds in roots.

Positron Imaging Used to Trace Radiolabelled Sugars in Plants

Several studies have used $[^{18}\text{F}]\text{fluorinated}$ sugar analogues (mainly $[^{18}\text{F}]\text{FDG}$) to visualize carbon dynamics in plants, providing an alternative methodology to $^{11}\text{CO}_2$ for tracing photoassimilate partitioning. Whereas sugars in plants are generated from photoassimilated carbon, $[^{18}\text{F}]\text{FDG}$ is a physicochemical and biochemical sugar analog, and thus is a surrogate tracer for movement of sugars in plants. The earliest report of $[^{18}\text{F}]\text{FDG}$ application and imaging in plants was by Hattori et al. in 2008.⁸² Here, the authors used a planar positron imaging system and radiographic imaging to quantify translocation of leaf-applied $[^{18}\text{F}]\text{FDG}$ through a sorghum plant (Figure 7A). From the applied leaf tip, $[^{18}\text{F}]\text{FDG}$ was translocated first to the discrimination center at the base of shoots, followed by redistribution to roots and young leaves. Accumulation was particularly pronounced at root tips.

Partelová et al. later used PET to image $[^{18}\text{F}]\text{FDG}$ uptake and transport in giant reed (*Arundo donax*) seedlings dosed through intact roots, damaged roots, excised stem, and cut leaf.⁸⁵ $[^{18}\text{F}]\text{FDG}$ uptake into plants was limited when applied through a cut leaf; however, the other dosing methods resulted in $[^{18}\text{F}]\text{FDG}$ accumulation in the plant. Roots were primary regions of accumulation in plants with roots (damaged or intact), but some $[^{18}\text{F}]\text{FDG}$ translocated to aboveground structures. Translocation was strongest in the reed plants' cut stems. PET was also used in another study that imaged $[^{18}\text{F}]\text{FDG}$ uptake into a tobacco leaf through an excised petiole immersed in solution. The authors found that increasing glucose concentration in the immersion solution enhanced diffusion and translocation into the leaf parenchyma tissues, and they speculated this was likely due to the accompanying increase in osmotic pressure.⁸⁶ A later study that also focused on $[^{18}\text{F}]\text{FDG}$ transport in tobacco leaf demonstrated rapid uptake, with radioactivity, measured by gamma spectrometry, reaching the leaf tip within 30 seconds (Figure 7B). PET scans showed that the initial uptake was dominated by the petiole and midrib, with slower movement into smaller veins likely governed by physicochemical forces.⁸⁴ Tobacco leaves were also the subject of a study by Best et al., in which radiographic imaging was used to visualize the intercellular exchange of newly acquired carbon ($[^{11}\text{C}]\text{CO}_2$) and root applied $[^{18}\text{F}]\text{FDG}$ in tobacco leaves of increasing age.⁸¹ Incorporation of root applied $[^{18}\text{F}]\text{FDG}$

decreased with leaf age, whereas [^{11}C] CO_2 incorporation into cellulose did not differ with leaf age. This suggests cellulose production in cell walls is limited by intercellular sugar exchange, rather than the developmental status of plant metabolic infrastructure. Results were reinforced by application of cellulose synthesis inhibitors, including methyl jasmonate and isoxaben.

Through tracing a specific radiolabelled compound, rather than an array of photoassimilates, detailed studies focusing on the metabolism and binding of sugars in plants have been used in conjunction with imaging. For example, in a recent study, the disaccharide sucrose was labelled with ^{18}F in different positions (1' and 6' substitutions in fructosyl and 6 in glucosyl moieties) by substituting hydroxyl groups and was then applied to wild and mutant maize leaf tips.⁸⁷ Radiography showed that the labelled analogues were transported similarly within respective wild and mutant maize plants, suggesting the hydroxyl groups removed from the sucrose did not bind with the ZmSUT1 transporter protein. Differences in transport rate were observed between wild and mutant type maize, with the mutant variety showing a greater transport rate relative to the wild. [^{18}F]FDS was also used in another study probing maize sucrose transporters through radiographic imaging.⁸³ Radiography imaged the movement of [^{18}F]FDS in leaves from wild type and *zmsut2* maize mutants, demonstrating that transport was equivalent. This result suggested that ZmSUT2 transporters do not play a role in leaf transport of sucrose, which contrasts with the previous study with ZmSUT1 mutants. It should be noted, that, despite the similarities in leaf sucrose transport behavior, *zmsut2* mutants accumulated more fructose, glucose, and sucrose in leaves than wild type maize.

A coupled radiographic/HPLC approach was used to probe [^{18}F]FDG allocation and metabolism in wounded-induced and methyl jasmonate-treated *Arabidopsis* (Figure 5C).²⁰ Transport of intact [^{18}F]FDG was in line with the spatially restricted vascular linkages of leaves to other sink structures in control plants. This partitioning pattern, however, was shifted in wounded-induced and methyl jasmonate-treated plants, where leaves treated or wounded received [^{18}F]FDG. HPLC analysis of leaf extracts showed possible incorporation of translocated [^{18}F]FDG into phenolic compounds, such as anthocyanin.

Positron Imaging for Visualization of Contaminant Dynamics in Plants

Tracers Used for Imaging Contaminant Metal Uptake and Translocation in Plants

A number of positron-emitting metal nuclides have been used to study plant uptake of toxic metals. These metals are either directly toxic to plants, causing biomass reduction (V, Zn) and/or inducing deficiency of other nutrients (V, Zn, Cd), or accumulate in plants and become available to other organisms to which metals are toxic (Cd, Zn). The most widely applied metal isotope used in the surveyed studies was ^{107}Cd , a radioactive

isotope of phytotoxic Cd. Within the context of toxicity rather than plant nutrition, the Zn isotope ^{62}Zn is also applicable to phytotoxicity studies. Positron-emitting nuclides of Cd and Zn are typically applied as divalent cations, providing the flexibility to modify these metals with ligands (e.g., siderophores, amino acids) of interest.

Positron-emitting ^{48}V for imaging plant is also available to study responses to V toxicity. Unlike Cd and Zn, V is generally used in an anionic form as protonated or polymerized VO_4^{3-} ions, with H_2VO_4^- and polymers (largely $\text{HV}_{10}\text{O}_{28}^{5-}$ and $\text{V}_4\text{O}_{12}^{4-}$) as the most favorable species at pH values relevant to plant studies (pH \approx 4–8). Within the context of phytotoxicity, ^{64}Cu has been used as well, albeit in only one study and in the form of [^{64}Cu]CuO nanoparticles.

Positron Imaging for Visualization of Plant Uptake and Translocation of Phytotoxic Metals

Early positron imaging studies with metal contaminants focused on V and Zn dynamics in plants. In one of these early studies, V uptake and translocation in cowpea was imaged using PETIS and radiographic imaging.²⁵ BAS radiographic imaging showed aboveground translocation of V occurring between 6 and 20 hours after exposure to V, before which V accumulated primarily in the roots. PETIS imaging of a trifoliate leaf structure showed faster and greater accumulation of V in the petiole of the leaf structure relative to the leaves.

Other early imaging studies probed the amelioration of V and Zn toxicity to rice and barley, respectively, by irradiated chitosan. Using radiographic imaging of a ^{48}V tracer in rice plants, Tham et al. determined that the presence of irradiated chitosan in the plant growth medium reduced translocation of V from roots to plant shoots.⁹⁵ The authors suggested that chitosan degraded by irradiation acts as a hormone-like mediator of V stress in rice. A similar effect was observed through PETIS imaging of barley under Zn stress grown in media with and without irradiated chitosan.¹⁰⁰ In this study, root to leaf translocation of Zn in barley was reduced by chitosan treatment of growth medium. In another study, accumulation of Zn tracer in specific *Arabidopsis* structures (i.e., silique, flower, cauline leaf, rosette leaf, and internode) was imaged using a real time radioisotope imaging system.⁹³ Zn was observed to be taken up and translocated. Although not a metal contaminant, it should be noted that this study also included imaging of positron-emitting ^{22}Na in the same tissues. Similarly, ^{22}Na was present in all tissues imaged.

Davis et al. used autoradiographic, PET/CT, and electron imaging approaches to study the uptake and translocation of functionalized, nanoparticulate [^{64}Cu]CuO by lettuce (*Lactuca sativa*).⁸⁸ Nanoparticles were observed to enter seedlings through the roots, where much of the ^{64}Cu accumulated, with some subsequent translocation to cotyledons. Dosing concentration of nanoparticles did not impact translocation within lettuce seedlings, but nanoparticle size did, with greater amounts of smaller (\approx 10 nm) nanoparticles taken up over a longer period of time relative to larger particles (\approx 20 nm).

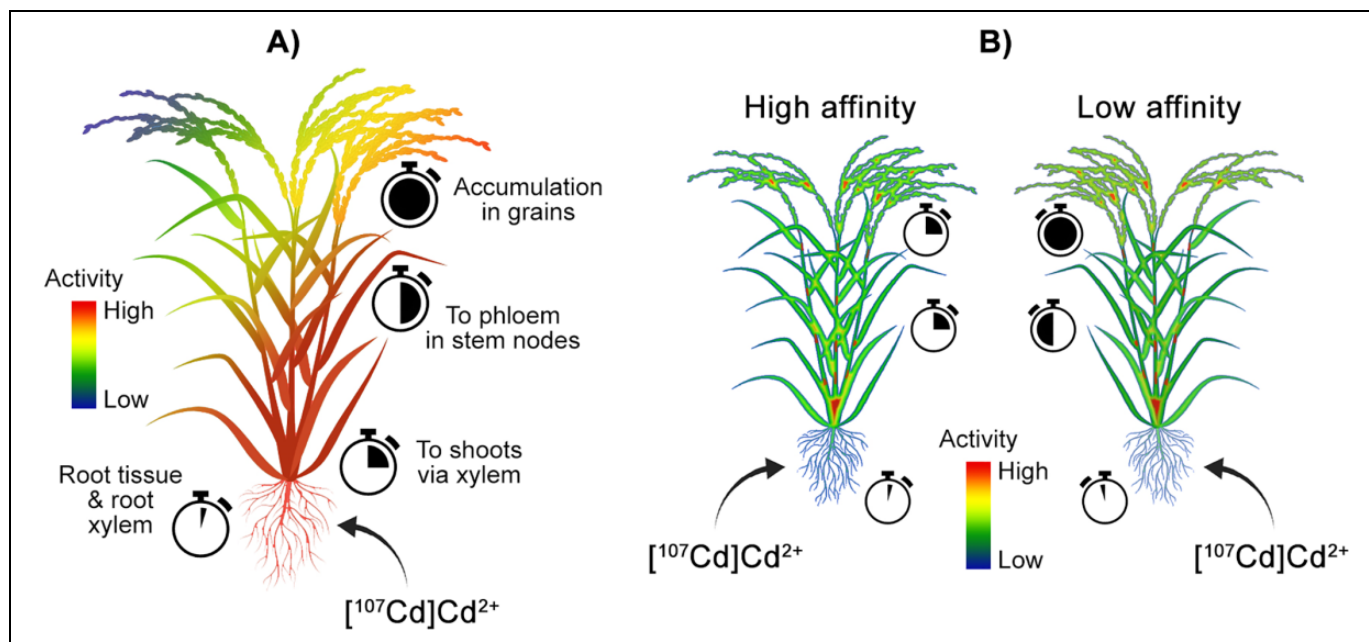


Figure 8. Examples of positron imaging of contaminant dynamics in plants. A) PETIS tracking of ^{107}Cd transport and allocation in rice.⁹⁰ Rice plants dosed with varying concentrations of ^{107}Cd at the roots transported Cd to root xylem and then to shoots via xylem, transferred Cd to the phloem at stem nodes, and finally to grains where Cd accumulated. Cd uptake rates were proportional to Cd concentrations. B) ^{107}Cd transport in high and low Cd affinity rice plants were studied using PETIS and autoradiography.⁹³ High-affinity plants transported Cd from roots to shoots much more rapidly relative to low-affinity plants.

Although not used as early as positron-emitting V and Zn tracers, ^{107}Cd has been extensively used as a tracer over the past decade. The first use of a ^{107}Cd tracer to follow plant uptake and translocation was reported by Fujimaki et al. in 2010 (Figure 8A).⁹⁰ In this study, Cd uptake and translocation were traced by PETIS from roots to grains in rice grown in media with different Cd concentrations. It was observed that uptake by roots was proportional to Cd concentration in the growth medium. The path of translocation started with absorption to root tissue followed by a shift to root xylem, transport to shoots via xylem, transfer to phloem in stem nodes, and transport to grains, where accumulation was observed.

In a later study, Cd uptake and translocation in 6 rice cultivars of differing Cd affinity (3 high and 3 low uptake cultivars) was investigated using PETIS and autoradiography (Figure 8B).⁹⁷ Cd uptake and translocation dynamics were observed between high and low affinity varieties, with high-affinity varieties demonstrating more rapid translocation of Cd from roots to shoots and panicles relative to low-affinity varieties. High-affinity varieties also showed a decrease of Cd in roots after peaking, whereas low-affinity varieties reached a plateau, corresponding with greater export elsewhere in the plant. The interactions between Zn and Cd and their influence on Cd uptake in rice was traced using PET and imaged by radiography.⁸⁹ Root to shoot translocation of Cd in rice appeared to be inhibited less by increasing Zn concentration than the inhibition of translocation of Zn by increasing Cd. This

suggests a Zn-insensitive transport Cd transport mechanism beyond the OsHMA2 Zn/Cd loading system previously identified.

Cd partitioning dynamics were also imaged in oilseed rape (*Brassica napus*) plants using PET.⁹³ Specifically, this study focused on the impact of glutathione and oxidized glutathione treatment on Cd uptake and translocation dynamics. Root treatment of glutathione reduced translocation from roots to shoots by reducing Cd concentration in roots and xylem transport of Cd. Reduction in root concentrations was linked to the increased Cd release from roots in response to the glutathione treatment. Similar inhibition was observed with the oxidized glutathione treatment.

Positron imaging has been used to study the uptake and translocation of Cd in known hyperaccumulator species. In one of these studies, PET and autoradiography were used to investigate the influence of nitrogen source (NO_3^- and NH_4^+) on Cd uptake, translocation, and extractability in a hyperaccumulator stonecrop species (*Sedum plumbizincicola*).⁹¹ Cd uptake and translocation was quicker and more extensive when plants were grown with NO_3^- , rather than ammonium, as the nitrogen source. The other reported imaging study of Cd in a hyperaccumulator species focused on the Asian common ladyfern (*Athyrium yokoscense*).⁹⁶ This plant showed large and reversible accumulation of Cd in distal roots and shoots under a basal nutrient growth medium. Translocation to shoots was suppressed, however, when the plant was grown in a nutrient-poor medium.

Table 4. Isotopes Used in Studies of Soils, Sediments, and Model Porous Media, With Half-Lives and Forms Used.

Isotope	Half-life	Form(s) used in imaging porous media
^{11}C	20.4 m	$[^{11}\text{C}]\text{CO}_2$ ¹¹⁴
^{18}F	109.8 m	$[^{18}\text{F}]\text{F}^-$ ^{116,119,120} $[^{18}\text{F}]\text{FDG}$ ^{115,117,118,112,113}
^{64}Cu	12.7 h	$[^{64}\text{Cu}]\text{Cu}^{2+}$, ¹¹⁶ $[^{64}\text{Cu}]\text{Cu}^{2+}$ -2-methyl-4-chlorophenoxyacetic acid (MCPA) ¹²⁰

Summary of Positron Imaging in Plant Sciences

Overall, positron imaging has been used extensively to yield many insights into plant processes. These approaches were used to study dynamics of water, essential macro- and micro-nutrients, and contaminants in various plant species and how these dynamics affect both above- and belowground processes. Furthermore, these topics have been investigated with positron imaging under a wide set of environmental conditions and variables, demonstrating the applicability of positron imaging to visualize plant responses to environmental changes and stresses. Positron imaging also serves as a novel bridge between different varieties of plant species (genetically modified or otherwise) and their subsequent phenotypic manifestations. These documented uses of positron imaging indicate the potential of positron imaging to serve as a powerful tool in real-time, whole-plant phenotyping, with respect to assessing critical factors in plant growth (e.g., nutrient and water partitioning behavior) and the effects of altering environmental variables (e.g., elevated temperature and CO_2 related to climate change) on plant growth.

Positron imaging has also demonstrated potential to enhance our understanding and exploitation of the complex relationships that exist between plants and the microorganisms that associate with them in the soil. There is a large body of literature that attests to the effects of certain plant growth promoting rhizobacteria, including significant increases in crop yield in an agricultural context.^{47, 104-111} Yet, to this day we still know little about the underlying mechanisms for these actions. As life is dynamic in nature, involving a constant ebb and flow of resources above and belowground, radioisotope-based imaging may be a powerful tool enabling researchers the opportunity to unravel these important interactions and mechanisms.

Positron Imaging—Soils and Sediments

Despite its prevalence in plant and geological sciences, positron imaging has not been used as much to study soils and sediments. Of the papers surveyed, PET was the only method of positron imaging used to study porous environmental media (i.e., soils, sediments, and model systems). This is likely because PET has many advantages over the other positron imaging approaches, PETIS or radiography, for these applications due to the density and geometry of soil and sediment samples, which may result in greater attenuation of positrons and sample thicknesses not suitable for radiography and

PETIS, respectively. . PET is also capable of time-resolved flow and biological activity imaging in cores and can visualize processes in these inherently opaque media. Because of these advantages, PET has been used with a selection of positron-emitting nuclides to study biotic activity in soils and sediments¹¹²⁻¹¹⁴ and transport of water¹¹⁵⁻¹¹⁹ and solutes^{116,120} in abiotic porous media (Tables 4 and 5). Although PET does not rival CT or magnetic resonance methods in terms of spatial resolution, studies have used these analyses in conjunction with PET to link dynamic radioisotope tracing with higher resolution structural details in soil, sediment, and model cores. Below, we summarize the application of radionuclides as tracers to visualize transport and metabolic processes in soils, sediments, and model porous media through PET imaging. Soils and sediments are highlighted here, as they are more intimately linked with biological processes in environmental systems relative to geological media (e.g., rocks). For a thorough review of PET applications and experimental considerations in geological systems, the reader is referred to Zahasky et al.¹⁵ and Kulenkampff et al.¹²¹

Positron Imaging for Visualization of Transport Processes in Porous Environmental Media

Tracers Used for Imaging Transport in Soils, Sediments, and Model Porous Media

Two ^{18}F labelled compounds have been used to image water transport in model and natural soils and sediments: $[^{18}\text{F}]\text{F}^-$ and $[^{18}\text{F}]\text{FDG}$. However, $[^{18}\text{F}]\text{F}^-$ and $[^{18}\text{F}]\text{FDG}$ differ in physicochemical properties from water, which may limit their usefulness as analogs for water movement. Given its inherently negative charge, F^- ions may be attracted electrostatically to matrices rich in Fe- and Al-oxides and other positively charged particles, potentially hindering its transport and, thus, its utility to monitor water flow in these systems. On the other hand, $[^{18}\text{F}]\text{FDG}$ is uncharged at environmentally relevant pH values and lacks any functional groups, which may reduce specific interactions with minerals common in soils and sediments. $[^{18}\text{F}]\text{FDG}$ may, however, be metabolized by organisms in the soil or sediment sample, making it a less than ideal tracer for water movement in systems where microbial activity is likely.

At this point, water transport has been studied more than solute transport; with both solute transport studies using ^{64}Cu

Table 5. Summary of Positron Imaging Experiments Focused on Soils/Sediments.

Area of study	Focus of study	Nuclide imaging modality	Reference(s)
Positron imaging for visualization of transport processes in porous environmental media			
<i>Positron imaging of transport processes in natural and model porous systems</i>	Imaging heterogeneous water flow in sand column	PET	118
	Water flow through sand core with and without flow impediments	PET	115, 119
	Water flow through a drill core composed of varying size sand, silt, gravel and coal particles	PET	116
	Water flow through a column of packed glass beads	PET	117
	Movement of Cu^{2+} through a sand column	PET	116
	Transport of Cu^{2+} -MCPA acid complex through a model soil column	PET	120
Positron imaging of biological activity in soils and sediments			
<i>Positron imaging for visualization of biological activity in natural and model porous systems</i>	Visualizing activity distribution of the bacterium <i>Rahnella</i> in a soil core layered with coarse and fine sections	PET	112
	Distribution of incipient active microbial communities in a floodplain sediment	PET	113
	Distribution of active autotrophic cyanobacteria across a biological soil crust	PET	114

in some form. Given the stability of Cu^{2+} ions in solution, Cu lends itself well to being used with or without a complexing agent. The literature reflects this, with one study using $[\text{}^{64}\text{Cu}]\text{Cu}^{2+}$ applied without a complexing agent and another using ^{64}Cu complexed with the herbicide MCPA. MCPA was selected in this study, as it is considered a contaminant with moderate leaching potential and also interacts with Cu and, thus, the radiotracer used in the respective study (^{64}Cu).

Positron Imaging of Transport Processes in Natural and Model Porous Systems

In 1998, Khalili et al. reported the first documented use of positron imaging for visualizing transport in a porous column study,¹¹⁸ where they imaged $[\text{}^{18}\text{F}]\text{FDG}$ distribution in 2 and 3 dimensions within a column of sandy sediment over 180 minutes. Specific regimes of near-wall flow were identified near the external portions of the column, leading to relative $[\text{}^{18}\text{F}]\text{FDG}$ depletion in these areas. This demonstrated that PET imaging can resolve heterogeneous water flow processes in sediment cores. In 2002, another study examined localized flow heterogeneity in a model sand column with various introduced flow impediments, including a clay layer and plastic inserts (e.g., spherical, cylindrical, and rectangular structures).¹¹⁹ This study used PET to visualize the zones of wall flow and the stagnation of flow around the introduced clay lens. PET was also used to quantify localized flow velocity measurements, demonstrating that PET can be used to quantifying regional flow parameters.

Flow around an obstructing object in a sand column was also modeled numerically and probed experimentally in a 2012 study (Figure 9A).¹¹⁵ Here, PET was used to image $[\text{}^{18}\text{F}]\text{FDG}$ movement in a sand column with and without a small cylindrical insert. The results aligned well with the Navier-Stokes

equation for flow of a viscous fluid in a porous medium. Water flow through a heterogeneous drill core consisting of fine sand, silt, gravel, and coal pieces was modeled using PET imaging of a $[\text{}^{18}\text{F}]\text{F}^-$ tracer.¹¹⁶ Localized flow parameters, such as flow velocity and mass flow were determined across cross-sections of the core. Similarly, a 2017 study used PET to image water in a model porous column packed with glass beads.¹¹⁷ Combined micro-CT imaging of packed cores and real-time water distribution from PET was used to visualize gravity-driven flow in the large pores of the packed column, and determine the permeability and porosity of cores.

PET was first applied to the transport of solutes in 2007 by Gründig et al., who used positron-emitting $[\text{}^{64}\text{Cu}]\text{Cu}^{2+}$ to track Cu flow and retention in a sand column.¹¹⁶ Cross-sectional flow velocities and Cu mass flows were visualized, demonstrating heterogeneous Cu flow within the column. Reversible retention of Cu was identified by similarity of Cu behavior to the conservative Br^- tracer used in other experiments. An irreversibly adsorbed fraction of Cu was also observed, identified through regions of decay-corrected activity values resistant to elution. This work demonstrated the application of PET for spatial visualization of contrasting adsorption processes.

A later study also focused on Cu transport in porous media, using a model soil column composed of sand- and silt-sized quartz coated with goethite (as a reactive solid phase) and illite (Figure 9B).¹²⁰ A radiolabelled $[\text{}^{64}\text{Cu}]\text{Cu}$ -MCPA complex showed slowed movement relative to a $[\text{}^{18}\text{F}]\text{F}^-$ tracer, suggestive of Cu-MCPA complex interaction with goethite. Despite this interaction with the goethite-coated packing material, breakthrough of Cu-MCPA complexes was observed within 66 hours. This study is also noteworthy for its use of batch adsorption studies and molecular speciation calculations to predict Cu-MCPA behavior.

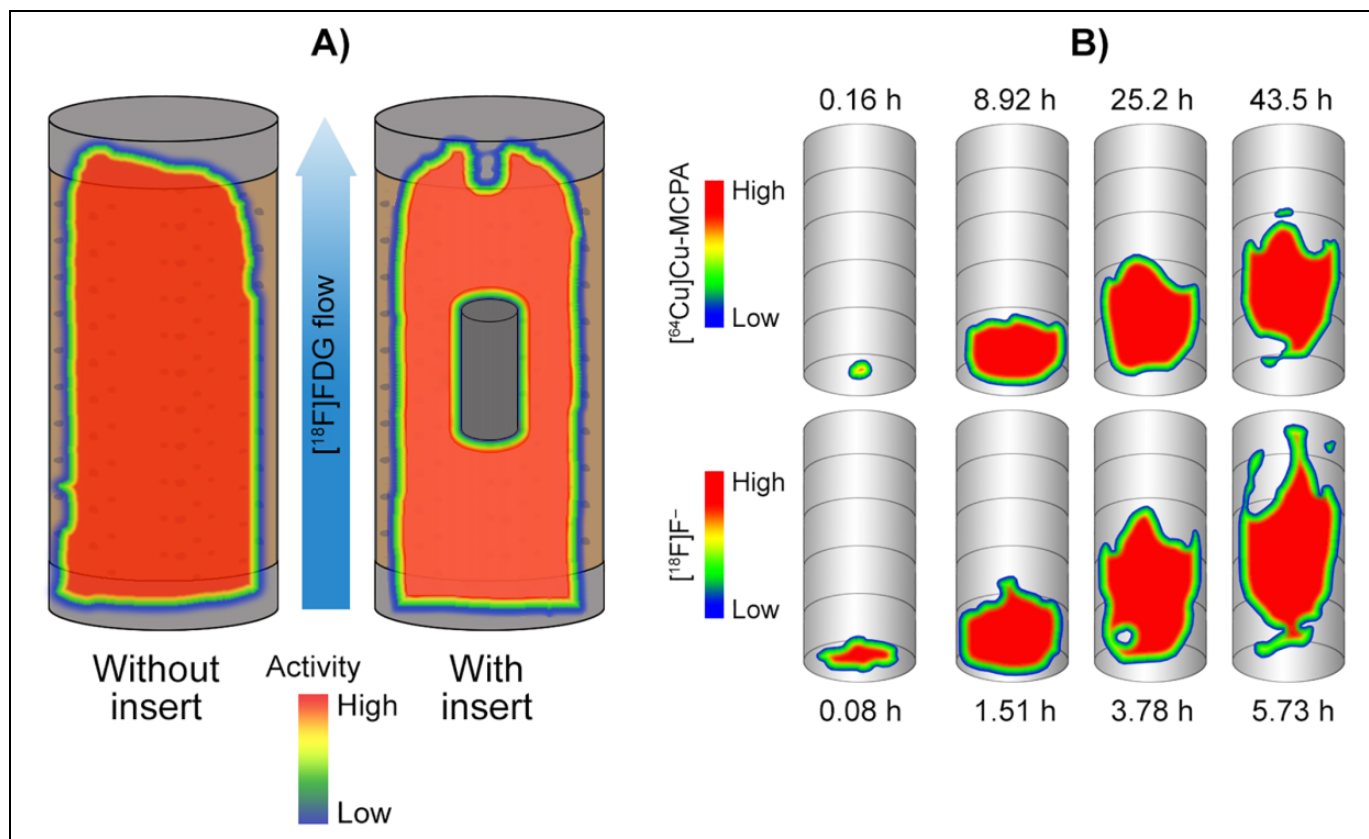


Figure 9. Examples of positron imaging of fluid transport processes in soil. A) Flow within a sand column with and without a cylindrical obstruction was imaged using positron emission tomography (PET) of [¹⁸F]FDG.¹¹⁵ B) PET imaging of ⁶⁴Cu and ¹⁸F in porous media consisting of sand- and silt-sized quartz coated with goethite and illite.¹²⁰ [⁶⁴Cu]Cu-MCPA complex moved slowly relative to a [¹⁸F]F⁻, which suggests Cu-MCPA interaction with goethite. A, B) Flow was driven from the bottom-up to reduce preferential flow channels and flow fingering and to allow escape of any gases formed during reactive flow. The PET imagery in A) was adapted from the *Journal of Applied Physics*, 76, Boutchko R, Rayz VL, Vandehey NT, O'Neil JP, Budinger TF, Nico PS, Druhan JL, Saloner DA, Gullberg GT, & Moses WW, Imaging and modeling of flow in porous media using clinical nuclear emission tomography systems and computational fluid dynamics, 74-81, Copyright (2012), with permission from Elsevier. The graphics in B were adapted from Ref.¹²⁰ under Creative Commons Attribution International License CC BY 4.0 (<https://creativecommons.org/licenses/by/4.0/>).

Positron Imaging of Biological Activity in Soils and Sediments

Tracers Used for Imaging Biological Activity in Porous Environmental Media

Of the studies surveyed here, 3 focused on microbiological activity in porous environmental media. Two of these studies visualized distribution of heterotrophic activity, and one imaged distribution of an autotrophic process. The 2 studies focusing on heterotrophic processes both used [¹⁸F]FDG as a tracer. Using [¹⁸F]FDG to the study of heterotrophic microbial metabolism assumes that the microbes' ability to metabolize glucose corresponds with their metabolism of [¹⁸F]FDG. Whether similar pathways are followed in [¹⁸F]FDG and glucose metabolism has yet to be fully explored. Although the metabolism of [¹⁸F]FDG by microbes is not entirely understood, studies that have used [¹⁸F]FDG to visualize microbial activity in soils and sediments have shown retention of ¹⁸F by active microbiota after exposure to [¹⁸F]FDG. This suggests

[¹⁸F]FDG may serve as an effective spatial label for heterotrophic microbiological activity in soils and sediments.

In studies examining autotrophic microbial processing in porous environmental media, [¹¹C]CO₂ has been the only label used to date. Although [¹¹C]CO₂ has been used as a spatial label for photosynthesis, its use should be carefully considered in soils and sediments, as it may be abiotically retained by soils and sediments.¹¹⁴ Specifically, investigators need to account for the partitioning of [¹¹C]CO₂ into water, which will provide a high background at most environmentally relevant pH values.

Positron Imaging for Visualization of Biological Activity in Natural and Model Porous Systems

The feasibility of using [¹⁸F]FDG as a tracer for microbial activity in soils was first explored by Kinsella et al., wherein the distribution of *Rahnella* activity within a simulated soil core was of interest.¹¹² After tracking water flow through simulated soil

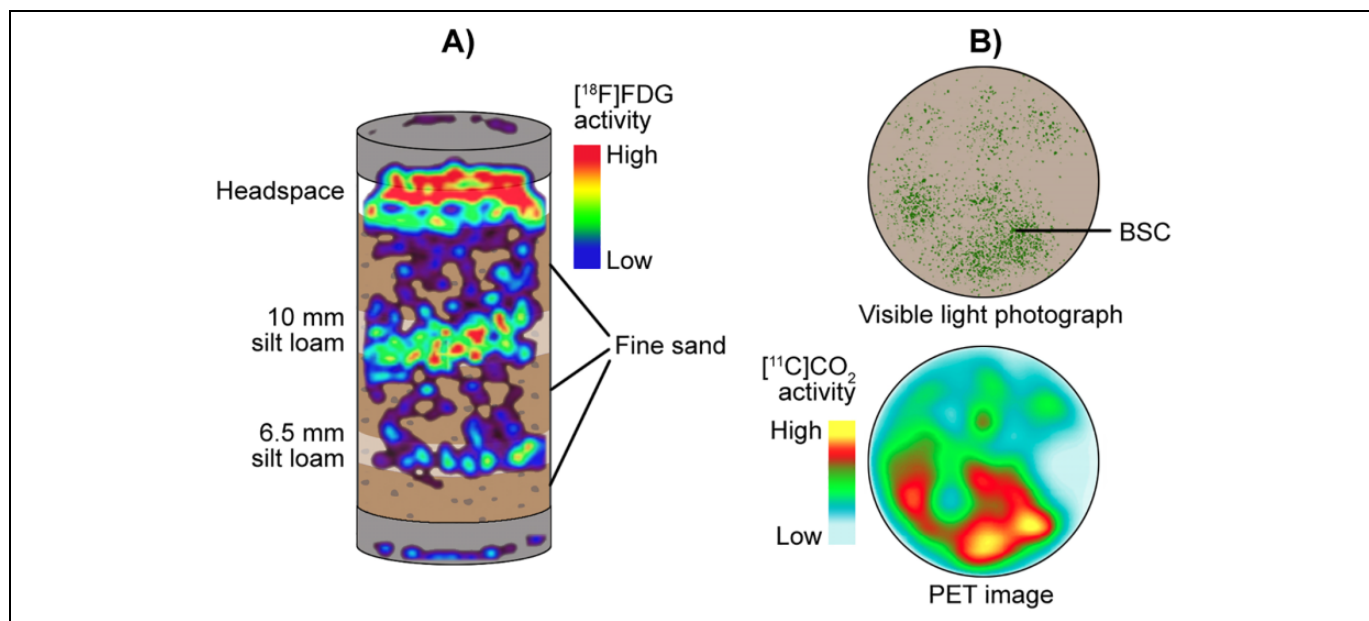


Figure 10. Examples of PET imaging of heterotrophic and autotrophic activity in porous and natural systems. A) Positron emission tomography (PET) imaging of *Rahnella* sp. Y9602 activity using [^{18}F]FDG applied to silt loam layers interspersed with sterile fine sand layers in a synthetic soil column.¹¹² Radioactivity in the inoculated silt loam layers was greater than within sterile sands, suggesting that biological activity associated with live cells was responsible for [^{18}F]FDG retention. B) PET imaging of [^{11}C]CO₂-inoculated biological soil crusts (BSC).¹¹⁴ PET activity distribution was positively correlated with green areas in photographs, suggesting a spatial relationship between cyanobacteria and CO₂ fixation. The PET imagery in A) was adapted from the *Journal of Hazardous Materials*, 213-214, Kinsella K, Schlyer DJ, Fowler JS, Martinez RJ, & Sobecky PA. Evaluation of positron emission tomography as a method to visualize subsurface microbial processes, 498-501, Copyright (2012), with permission from Elsevier. The PET image in B) was adapted with permission from Vandehey NT, Northen TR, Brodie EL, & O'Neil JP, 2014, Noninvasive mapping of photosynthetic heterogeneity in biological soil crusts by positron emission tomography: carbon fixation. *Environmental Science and Technology Letters*, 1(10), 393-398. Copyright (2014) American Chemical Society.

using an [^{18}F]F⁻ tracer, the authors verified the ability to spatially resolve bacterial colonies by using activated carbon adsorbents placed throughout the core, which retained radiolabelled [^{18}F]FDG and served as a spatial probe for [^{18}F]FDG retention. The distribution of *Rahnella* was then spatially resolved within a sand core banded with silt loam, with activity concentrated near the silt loam band, indicating retention by or colonization of these more finely textured materials (Figure 10A). Activity in banded cores inoculated with active cells was greater than activity in sterile banded cores and banded cores inoculated with autoclaved cells, suggesting biological activity associated with live cells was responsible for retention of [^{18}F]FDG.

The other study probing spatial distribution of heterotrophic microbial activity in natural porous media investigated distribution of [^{18}F]FDG flow and incipient microbial communities in a floodplain sediment.¹¹³ Active microbiota in sediments pre-treated with glucose for 10 days were observed by PET to increase the retained activity of added [^{18}F]FDG relative to sterile sediment, sand, and a sand column with flow-disrupting inserts. These results were coupled with 16S rRNA analyses, which showed a shift in microbial community after glucose pre-treatment. Microbial community within the active sediment, however, showed little variation between depths across the probed 16-cm core.

In addition to these 2 studies using PET to visualize distribution of heterotrophic microbial activity in soils and sediments, another study focused on the distribution of autotrophic cyanobacterial activity, in the form of photosynthetic fixation of [^{11}C]CO₂, in biological soil crusts under different watering regimes.¹¹⁴ Spatial heterogeneity of photosynthetic activity across biological soil crusts was imaged using PET. Comparison of PET activity distribution with photographs of the crusts revealed a positive correlation between green areas and active photosynthetic fixation (Figure 10B). A general link was found between wetting and photosynthetic activity, with wetting increasing surface photosynthetic uptake of [^{11}C]CO₂, likely due to hydrotaxis by autotrophic cyanobacteria in response to wetting.

Summary of Positron Imaging in Porous Environmental Media

Despite the modest number of studies applying positron imaging to porous environmental and model media (relative to plant-based studies), reported studies represent a topically and methodologically diverse base of research. PET has proven to be a useful tool for the visualization of water and solute flow in environmental media. Porous media included cores of natural

materials and model porous media (e.g., sand, glass beads). Additionally, PET has been applied to the non-invasive spatial resolution of biological activity in soils and sediments, a perspective not accessible to researchers by other existing methodologies. With complementary imaging approaches, such as CT, regions of physical or biological interest have been linked with inherent structural features in these systems, providing a unique, non-destructive bridge between active processes and structure in environmental media. Together, these results demonstrate the capacity and value of positron imaging for visualizing a range of physical and biogeochemical processes in soils and sediments.

Soil biogeochemical processes are often driven by the exchange of soil nutrients and contaminants between soil microbiota and their surrounding soil habitats. Much, however, remains to be known about the spatial relationships that govern microbial activity distribution in soils. Given previous findings, which highlight differences in microbial community between macro- (>250 μm) and microaggregate (<250 μm) size fractions in soils, it is subsequently critical to identify how these community differences translate to activity across these spatial scales to further unravel relationships driving key soil biogeochemical processes (e.g. respiration, contaminant transformation, carbon storage).¹²²⁻¹²⁴ These scales are within the spatial resolution of PET (large macroaggregates) and autoradiography (macro- and microaggregates), highlighting the unique potential of these approaches to explore the role of spatial heterogeneity in soil biogeochemical processes.

Positron Imaging in Environmental Sciences Future Directions

Future research applications of positron imaging in the environmental sciences will likely draw from a variety of influences, including application and development of novel tracers, a broader base of plant species, ecological interactions between species, dynamics at the plant/soil/microbe interface, and advancements in coupling positron imaging with other analyses. Through these directions, and others yet unknown, positron imaging will continue to provide insight into critical environmental processes.

Potential Tracers for Future Positron Imaging Studies

A number of positron-emitting tracers are currently available that have yet to be imaged in an environmental context. This includes a variety of organic molecules that could serve as novel probes for plant physiological studies, such as gases (e.g., [^{11}C]methane),¹²⁵ labelled amino acids (e.g., [^{11}C]leucine, [^{11}C]tyrosine, and [^{18}F]glutamine),¹²⁶⁻¹²⁹ sugars (e.g., [^{11}C]glucose, [^{11}C]fructose, and [^{11}C]sucrose),¹²⁹ and other biochemical building blocks (e.g., [^{11}C]choline and [^{11}C]pyruvate).^{130,131} These tracers may also promote further studies in imaging microbial processing in soils and sediments, allowing researchers to access processes beyond glucose metabolism in

these systems. In addition to these established tracers having a potential impact on future environmental positron imaging studies, synthetic routes for tagging molecules with positron-emitting nuclides continue to be developed, particularly with ^{18}F and ^{11}C . Accordingly, the ability to tailor specific organic molecules for the purposes of studying environmental processes will likely improve as well.

Many inorganic positron-emitting isotopic tracers remain unexplored in environmental systems. Of particular relevance to the topics covered here are ^{55}Co ($t_{1/2} = 17.5$ hours), ^{56}Co ($t_{1/2} = 77.2$ days), ^{58}Co ($t_{1/2} = 70.9$ days), ^{72}As ($t_{1/2} = 26$ hours), ^{83}Sr ($t_{1/2} = 32.4$ hours), and $^{94\text{m}}\text{Tc}$ ($t_{1/2} = 53$ minutes).¹³² These elements are environmental contaminants whose transport and fate in soils and sediments could be probed with positron imaging. Positron imaging could also be used to study the uptake and translocation of these elements in plants. As with metals previously applied in environmental studies, use of appropriate chelating agents may make these tracers suitable for future work in visualizing dynamics of inorganic environmental contaminants in plants, soils, and sediments. In addition to these inorganic species, there are numerous organic compounds that may be labelled with positron emitting isotopes. This includes labelling with ^{11}C , ^{18}F , and ^{124}I ($t_{1/2} = 4.2$ days).¹³³⁻¹³⁵ Molecules with these incorporated labels could potentially span a range of biochemical classes in plants and soil microbiota as well as prominent organic contaminants. As with other tracers discussed previously, the similarity in behavior of tagged molecules with respect to untagged molecules should be considered.

Future Directions in Positron Imaging of Plants

Many of the published studies applying positron imaging to plants are focused on species of agricultural and horticultural significance. Given the ongoing, pressing need for agricultural intensification in an increasingly stressed environment, using positron imaging for precision phenotyping of agriculturally relevant crops will likely continue developing. Particularly relevant will be studies using positron imaging to visualize plant responses (e.g., internalization and translocation of water, nutrients, and photoassimilates) to environmental conditions projected to shift with climate change, including varying temperature and moisture regimes. Additionally, positron imaging has the potential to be an important phenotyping tool for plant breeders focused on these challenges, with rapid visualization of different plant varieties in real-time serving as a guide for traits under a changing environment. The ability to dose and image multiple plants simultaneously also has the potential to increase the throughput of phenotyping by positron imaging, further enhancing the applicability of positron imaging approaches to plant phenotyping.

In addition to studying plants in agricultural environments, positron imaging can also be used to study plants in unmanaged ecosystems. Although plant species from unmanaged environments have not been the subject of as many positron imaging studies as agriculturally relevant species thus far, there is great potential for positron imaging to further probe plant dynamics

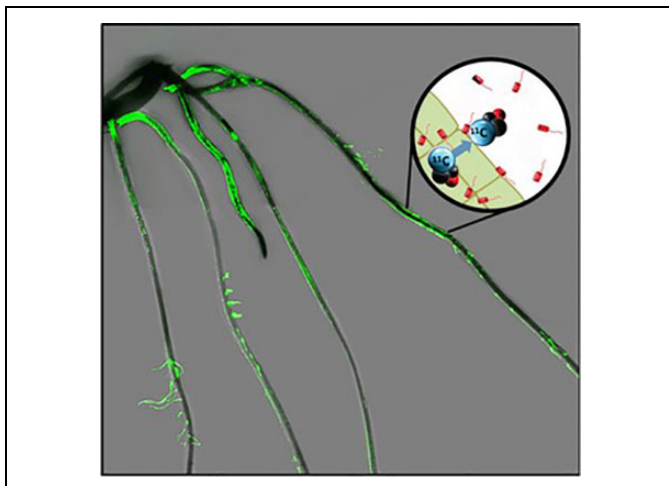


Figure 11. Plant-borne carbon tracing to root associating rhizobacteria. Atmospheric carbon is traced from plant fixation of radioactive $[^{11}\text{C}]\text{CO}_2$ through root translocation as complex $[^{11}\text{C}]$ photoassimilates. There, this carbon source is assimilated by root-associating microorganisms. This overlay of images from ^{11}C -radiography (dark black regions reflect high levels of ^{11}C activity) and a green fluorescence image arising from RAM10, a GFP reporting strain of *H. seropedicae* bacteria demonstrates that regions of high root colonization seem to draw more ^{11}C .

in present environments and to project behavior under climactic changes as well. This could potentially include whole-plant imaging studies of wild grasses, bushes, and developing trees, as well as structure-specific studies of species too large to image on a whole-plant scale with current imaging approaches.

The spatial relationships accessible with positron imaging are also compatible with studying plant-plant and other ecological interactions within rooting systems. Areas of research focused on mycorrhizal associations and root parasitic plant species would benefit from the visualization of resource (e.g., nutrients, sugars) transfer by positron imaging. Non-destructive visualization of resource dynamics in spatially associated structures would provide a novel viewpoint on rhizosphere ecology, particularly if combined with high resolution CT or MRI imaging.

A recent example of using positron imaging with a complementary imaging approach to trace photoassimilate flow to root associated bacteria is reported by Waller et al.¹³⁶ Here, researchers demonstrated that radioactive $[^{11}\text{C}]\text{CO}_2$ administered to intact maize leaves translocated as $[^{11}\text{C}]$ photoassimilate preferentially to roots that had a high density of root associating bacteria. They used fluorescence root imaging of RAM10, a green fluorescent protein (GFP) reporting strain of *H. seropedicae*, to identify regions of high microbial colonization and correlate those regions with levels of ^{11}C -activity using radiography (Figure 11). Use of ^{11}C provided a “traceable” source of carbon whose assimilation by microbial organisms was quantifiable with enormous sensitivity.¹³⁶

Future Applications of Positron Imaging to Soils and Sediments

Studies show that positron imaging is a useful tool for probing key biotic and abiotic processes in soils and sediments. Potential future areas of investigation with positron imaging include visualization of abiotic processes, such as localized accumulation of contaminants (organic and inorganic), retention of natural organic matter, and nutrient fate in soil samples. Potential biotic processes that may be probed with positron imaging include biomineralization processes, metabolism of radiolabelled substrates, and microbial interaction with organic and inorganic contaminants.

Role of Complementary Analyses in the Future of Positron Imaging

In 2014, Vandehey et al. were the first to acknowledge the utility of non-destructive positron imaging as a spatial guide for further chemical and biological analysis in biogeochemical systems.¹¹⁴ The millimeter-scales probed by PET, for example, are between bulk-scale measurements of soils and finer-scale measurements, highlighting the relevance of PET to link processes across scales. This potential of positron imaging to guide biological analyses has been utilized for spatial delineation of microbial community analysis.¹¹³ Future research efforts with positron imaging in soils will be able to build on this concept, providing a targeted characterization of biogeochemical activity in soils.

Positron imaging also has the potential to characterize active microbial communities associated with plants, serving as a spatial link between active resource exchange and plant-associated microbial community composition. In addition, positron imaging may also improve biochemical speciation (e.g., metabolomic and proteomic profiles) of microbial communities in these environments, using localized activities as a spatial reference for extraction procedures. Used in conjunction with a suite of available radiochemical tracers, positron imaging will develop as an important tool for understanding spatial relationships between microbiota and their localized habitats in environmental systems.

Complementary chemical analyses, particularly those with high-resolution imaging compatibility, may in the future serve as an important interface with positron imaging measurements in plants, soils, and sediments. After identifying regions of biogeochemical activity using positron imaging, zones of interest may be further analyzed using a toolbox of spectroscopic analyses to probe local chemical environments. This includes infrared microspectroscopy, which analyzes molecular vibrations to identify environmentally relevant species, such as biomolecules and minerals, with spatial resolution (optimally $\approx 3\ \mu\text{m}$, but dependent upon wavelength) exceeding positron imaging approaches at smaller sampling areas (up to a few hundred micrometers).¹³⁷ Further, application of synchrotron-based X-ray microprobes for X-ray fluorescence imaging (XFI), X-ray absorption spectroscopy (XAS), and X-ray diffraction (XRD)

at spatial resolution of 0.1 (with zone plates) to 10 μm^2 on mm^2 sample areas may provide insight into chemical speciation and mineralogy of specific spots of samples of interest as identified by PET or autoradiography. Furthermore, techniques such as scanning transmission X-ray microscopy (STXM), can provide elemental mapping and elementally specific local chemical environment for light elements (especially carbon and nitrogen) with sub-micron spatial resolution and may prove to be a valuable complement to future positron imaging studies.¹³⁸ Another tool for mapping elemental distribution with high resolution (generally $\approx 5\text{--}200\ \mu\text{m}$ is attainable) is laser ablation inductively coupled plasma mass spectrometry (LA-ICP-MS).⁸ This technique makes use of a focused laser beam to ablate samples, with ablated material subsequently directed into an ICP-MS, where a variety of elements are simultaneously quantified with detection limits typically ranging from 0.001–1 $\mu\text{g g}^{-1}$ of sample. Additionally, specific isotope distributions are detectable with LA-ICP-MS, providing a high-resolution, quantitative distribution of a variety of metals and specific metal isotopes in environmental samples.

From a mass spectrometric approach, application of positron-emitting radionuclides in conjunction with certain stable isotopes (e.g., ^{13}C , ^{15}N) to a soil or plant could permit further tracing with higher resolution by a mass spectrometric imaging technique, like nanoscale secondary ion mass spectrometry (nanoSIMS), which can provide spectrograms of fragment masses through a focused ion beam from 50–150 nm in diameter.^{139,140} Mass-based characterization of added stable nuclides could provide a novel viewpoint on localized biogeochemistry within active regions identified by positron imaging in plants and soils. nanoSIMS has been used previously in plant and soil systems, with special attention to sample preparation required for both sample types.^{101,139,141} The reader is referred to these sources for further information regarding appropriate sample preparation and technical details regarding nanoSIMS analysis. Other possible complimentary mass spectrometric imaging approaches include laser ablation mass spectrometric imaging by matrix assisted laser desorption ionization (MALDI) and laser ablation electrospray ionization (LAESI) mass spectrometry. These approaches have potential to interface with positron imaging through spatially mapping plant metabolites within regions identified through accumulation of radioactivity, with cell-scale measurements possible.¹⁴²

Maximizing the complementary use of these spectrometric and spectroscopic methods with positron imaging is dependent on appropriately linking areas identified by positron imaging and the smaller regions generally probed with the complementary analyses. A combination of imaging approaches could help bridge this gap, particularly in the case of PET, which generally has a lower spatial resolution than autoradiographic imaging. Researchers attempting to apply high resolution spectroscopic analyses to regions identified in environmental samples by PET may want to include an autoradiographic imaging component to better define a region of activity more compatible with smaller regions of interest probed by complementary analyses. It is also possible that CT or MRI imaging could be used in

conjunction with PET to unequivocally identify specific structures associated with tracer dynamics; this could be used to image a more restricted and relevant region of interest for a higher resolution study (e.g., a fine root clearly resolved by CT linked with a broader zone of activity as observed by PET), while retaining the 3-dimensional volumes not available with autoradiography.^{22,43}

With these possible avenues, positron imaging is poised to play an important role in the future of environmental sciences. Through application of new tracers, new processes in plants and soils will be made accessible to positron imaging. Incorporating new plant species, ecological interactions, and environmental conditions will provide new scenarios where positron imaging may be used. Positron imaging will benefit from innovative use of complementary biological and chemical speciation, serving as a spatial link between biogeochemical activity and both bulk and molecular measurements, allowing for a more holistic understanding of spatial relationships within inherently heterogeneous environmental systems.

Acknowledgments

M.P.S. would like to acknowledge the Natural Sciences and Engineering Research Council Collaborative Research and Training Experience Sustainable Applied Fertilizer and Environmental Remediation (NSERC CREATE SAFER) program and a Natural Sciences and Engineering Research Council Collaborative Research and Development grant supported by Federated Cooperatives Limited for financial support.


Declaration of Conflicting Interests

The author(s) declared no potential conflicts of interest with respect to the research, authorship, and/or publication of this article.

Funding

The author(s) disclosed receipt of the following financial support for the research, authorship, and/or publication of this article: The Natural Sciences and Engineering Research Council Collaborative Research and Training Experience Sustainable Applied Fertilizer and Environmental Remediation (NSERC CREATE SAFER) program and a Natural Sciences and Engineering Research Council Collaborative Research and Development grant supported by Federated Cooperatives Limited provided financial support (Grant Number 537285-18). Additional support was provided by the Sylvia Fedoruk Canadian Centre for Nuclear Innovation (Grant Number J2018-0041). This research was supported, in part by Agriculture and Food Research Initiative (Award Number 2017-67013-26216) from the USDA National Institute of Food and Agriculture and in part by Bayer Crop Science, Grants4Biologicals Program (Award Number 2019-01-035).

ORCID iD

Michael P. Schmidt  <https://orcid.org/0000-0001-8789-9204>

References

1. Ruben S, Hassid WZ, Kamen MD. Radioactive carbon in the study of photosynthesis. *J Am Chem Soc.* 1939;61:661–663.
2. McKay RML, Palmer GR, Ma XP, Layzell DB, McKee BTA. The use of positron emission tomography for studies of long-distance

- transport in plants: uptake and transport of ^{18}F . *Plant Cell Environ.* 1988;11(9):851–861.
3. Matsushashi S. Radiation-based plant diagnostics: positron imaging-based studies of plants. In: Kudo H, ed. *Radiation Applications*. 1st ed. Springer; 2018:255–292.
 4. L'Annunziata MF. Gamma- and X-radiation photons. In: L'Annunziata MF, ed. *Radioactivity: Introduction and History*. 1st ed. Elsevier; 2007:187–215.
 5. Phelps ME, Cherry SR, Dahlbom M. *PET: Physics, Instrumentation and Scanners*. Springer; 2006.
 6. Rich DA. A brief history of positron emission tomography. *J Nucl Med Technol.* 1997;25(1):4–11.
 7. Wagner HNJr. A brief history of positron emission tomography (PET). *Semin Nucl Med.* 1998;28(3):213–220.
 8. L'Annunziata MF. *Handbook of Radioactivity Analysis*. 3rd ed. Elsevier; 2012.
 9. Conti M, Eriksson L. Physics of pure and non-pure positron emitters for PET: a review and a discussion. *EJNMMI Physics*. 2016; 3(1):8.
 10. Bailey D, Karp J, Surti S. Physics and instrumentation in PET. In: Bailey D, Townsend D, Valk P, Maisey M, eds. *Positron Emission Tomography*. 1st ed. Springer; 2005:13–39.
 11. Jødal L, Le Loirec C, Champion C. Positron range in PET imaging: an alternative approach for assessing and correcting the blurring. *Phys Med Biol.* 2012;57(12):3931–3943.
 12. Levin CS, Hoffmann EJ. Calculation of positron range and its effect on the fundamental limit of positron emission tomography system spatial resolution. *Phys Med Biol* 1999;44(3):781–799.
 13. Levin CS. Primer on molecular imaging technology. *Eur J Nucl Med Mol Imaging.* 2005;32(Suppl 2):S325–S345.
 14. Zakhnini A, Kulenkampff J, Sauerzapf S, Pietrzyk U, Lippmann-Pipke J. Monte Carlo simulations of GeoPET experiments: 3D images of tracer distributions (^{18}F , ^{124}I , and ^{58}Co) in Opalinus clay, anhydrite and quartz. *Comput Geosci-UK.* 2013;57:183–196.
 15. Zahasky C, Kurotori T, Pini R, Benson SM. Positron emission tomography in water resources and subsurface energy resources engineering research. *Adv Water Resour.* 2019;127:39–52.
 16. Hubeau M, Mincke J, Vanhove C, et al. ^{11}C -autoradiographs to image phloem loading. *Front For Glob Change.* 2019;2:20.
 17. Babst BA, Ferrieri R, Schueller M. Detecting rapid changes in carbon transport and partitioning with carbon-11 (^{11}C). In: Liesche J, ed. *Phloem: Methods and Protocols*. 1st ed. Springer-Nature; 2019:163–176.
 18. Thorpe MR, Minchin PEH. In vivo veritas: radiotracers in studies of phloem transport of carbohydrate. In: Liesche J, ed. *Phloem: Methods and Protocols*. 1st ed. Springer-Nature; 2019:177–194.
 19. Weisenberger AG, Kross B, Lee SJ, et al. Nuclear physics detector technology applied to plant biology research. *Nucl Instrum Methods Phys Res A.* 2013;718:157–159.
 20. Alexoff DL, Dewey SL, Vaska P, et al. PET imaging of this objects: measuring the effects of positron range and partial-volume averaging in the leaf of *Nicotiana tabacum*. *Nuc Med Biol.* 2011;38(2):191–200.
 21. Ferrieri AP, Appel H, Ferrieri RA, Schultz JC. Novel application of 2- ^{18}F fluoro-2-deoxy-D-glucose to study plant defenses. *Nuc Med Biol.* 2012;39(8):1152–1160.
 22. Jahnke S, Menzel MI, Schur U. Combined MRI-PET dissects dynamic changes in plant structures and functions. *Plant J.* 2009;59(4):634–644.
 23. Wang Q, Komarov S, Mathews AJ, Li K, Topp C, O'Sullivan JA, Tai YC. Combined 3D PET and optical projection tomography techniques for plant root phenotyping. 2015; arXiv Preprint arXiv:1501.00242.
 24. Ferrieri RA, Herman E, Babst B, Schueller MJ. Managing the soil nitrogen cycle in agroecosystems. In: Lal R, Stewart BA, eds. *Advances in Soil Science Soil Nitrogen Uses and Environmental Impacts (Advances in Soil Science)*. 1st ed. CRC Press; 2018: 341–358.
 25. Furukawa J, Yokota H, Tanoi K, et al. Vanadium uptake and an effect of vanadium treatment on ^{18}F -labeled water movement in a cowpea plant by positron emitting tracer imaging system (PETIS). *J Radioanal Nucl Chem.* 2001;249:495–498.
 26. Kang DJ, Nakanishi TM, Kume T, Ishii R. Determination of ^{18}F -labeled water movement to the leaf and its association with water relations in acid soil-tolerant rice varieties. *J Crop Sci Biotech.* 2009;12(4):261–265.
 27. Kiyomiya S, Nakanishi H, Uchida H, et al. Light activates H_2^{15}O flow in rice: detailed monitoring using a positron-emitting tracer imaging system (PETIS). *Physiol Plant.* 2001;113(3):359–367.
 28. Kume T, Matsushashi S, Shimazu M, et al. Uptake and transport of positron-emitting tracer ^{18}F in plants. *Appl Radiat Isot.* 1997; 48(8):1035–1043.
 29. Mori S, Kiyomiya S, Nakanishi H, et al. Visualization of ^{15}O -water flow in tomato and rice in the light and dark using a positron-emitting tracer imaging system (PETIS). *Soil Sci. Plant Nutr.* 2000;46(4):975–979.
 30. Nakanishi TM, Okuni Y, Furukawa J, et al. Water movement in a plant sample by neutron beam analysis as well as positron emission tracer imaging system. *J Radioanal Nucl Chem.* 2003;255(1): 149–153.
 31. Nakanishi TM, Tanoi K, Yokota H, et al. ^{18}F used as tracer to study water uptake and transport imaging of a cowpea plant. *J Radioanal Nucl Chem.* 2001;249(2):503–507.
 32. Nakanishi TM, Yokota H, Tanoi K, et al. Comparison of ^{15}O -labeled and ^{18}F -labeled water uptake in a soybean plant by PETIS (positron emitting tracer imaging system). *Radioisotopes.* 2001; 50(6):265–269.
 33. Ohya T, Tanoi K, Hamada Y, et al. An analysis of long-distance water transport in the soybean stem using H_2^{15}O . *Plant Cell Physiol.* 2008;49(5):718–729.
 34. Tanoi K, Hojo J, Nishioka M, Nakanishi TM, Suzuki K. New technique to trace [^{15}O]water uptake in a living plant with an imaging plate and a BGO detector system. *J Radioanal Nucl Chem.* 2005;263(2):547–552.
 35. Tsukamoto T, Uchida H, Nakanishi H, et al. H_2^{15}O translocation in rice was enhanced by 10 μM 5-aminolevulinic acid as monitored by positron emitting tracer imaging system (PETIS). *Soil Sci Plant Nutr.* 2004;50(7):1085–1088.
 36. Bughio N, Nakanishi H, Kiyomiya S, et al. Real-time [^{11}C]methionine translocation in barley in relation to mugineic acid phytosiderophore biosynthesis. *Planta.* 2001;213(5): 708–715.

37. Hayashi H, Okada Y, Mano H, et al. Detection and characterization of nitrogen circulation through the sieve tubes and xylem vessels of rice plants. *Plant Soil*. 1997;196:223–237.
38. Ishii S, Suzui N, Ito S, et al. Real-time imaging of nitrogen fixation in an intact soybean plant with nodules using ^{13}N -labeled nitrogen gas. *Soil Sci Plant Nutr*. 2009;55(5):660–666.
39. Ishimaru Y, Kim S, Tsukamoto T, et al. Mutational reconstructed ferric chelate reductase confers enhanced tolerance in rice to iron deficiency in calcareous soil. *Proc Natl Acad Sci USA*. 2007;104(18):7373–7378.
40. Ishimaru Y, Suzuki M, Tsukamoto T, et al. Rice plants take up iron as an Fe^{3+} -phytosiderophore and as Fe^{2+} . *Plant J*. 2006;45(3):335–346.
41. Kasel MCK, Schueller MJ, Ferrieri RA. Optimizing ^{13}N radiochemistry for nitrogen-fixation in root nodules of legumes. *J Label Compd Radiopharm*. 2010;53(9):592–597.
42. Kiyomiya S, Nakanishi H, Uchida H, et al. Real time visualization of ^{13}N -translocation in rice under different environmental conditions using positron emitting tracer imaging system. *Plant Physiol*. 2001;125(4):1743–1754.
43. Liang W, Nie Y, Wang J, et al. Three-dimensional positron emission tomography/computed tomography analysis of $^{13}\text{NO}_3^-$ uptake and ^{13}N distribution in growing kohlrabi. *Anal Chem*. 2011;83(2):578–584.
44. Matsunami H, Arima Y, Watanabe K, et al. ^{13}N -nitrate uptake sites and rhizobium-infectible region in a single root of common bean and soybean. *Soil Sci Plant Nutr*. 1999;45(4):955–962.
45. Nakanishi H, Bughio N, Matsuhashi S, et al. Visualizing real time ^{11}C methionine translocation in Fe-sufficient and Fe-deficient barley using a positron emitting tracer imaging system (PETIS). *J Exp Bot*. 1999;50(334):637–643.
46. Ohtake N, Sato T, Fujikake H, et al. Rapid transport to pods and seeds in N-deficient soybean plants. *J Exp Bot*. 2001;52(355):277–283.
47. Pankievicz VCS, Do Amaral FP, Santos KFDN, et al. Robust biological nitrogen fixation in a model grass-bacterial association. *Plant J*. 2015;81(6):907–919.
48. Sato T, Ohtake N, Ohya T, et al. Analysis of nitrate absorption and transport in non-nodulated and nodulated soybean plants with $^{13}\text{NO}_3^-$ and $^{15}\text{NO}_3^-$. *Radioisotopes*. 1999;48:450–458.
49. Suzuki M, Tsukamoto T, Inoue H, et al. Deoxymugineic acid increases Zn translocation in Zn-deficient rice plants. *Plant Mol Biol*. 2008;66(6):609–617.
50. Tsukamoto T, Nakanishi H, Kiyomiya S, et al. ^{52}Mn translocation in barley monitored using a positron-emitting tracer imaging system. *Soil Sci Plant Nutr*. 2006;52(6):717–725.
51. Tsukamoto T, Nakanishi H, Uchida H, et al. ^{52}Fe translocation in barley as monitored by a positron-emitting tracer imaging system (PETIS): evidence for the direct translocation of Fe from roots to young leaves via phloem. *Plant Cell Physiol*. 2009;50(1):48–57.
52. Watanabe S, Iida Y, Suzui N, et al. Production of no-carried-added ^{64}Cu and applications to molecular imaging by PET and PETIS as a biomedical tracer. *J Radioanal Nucl Chem*. 2009;280(1):199–205.
53. Agtuca B, Rieger E, Hilger K, et al. Carbon-11 reveals opposing roles of auxin and salicylic acid in regulating leaf physiology, leaf metabolism, and resource allocation patterns that impact root growth in *Zea mays*. *J Plant Growth Regul*. 2014;33(2):328–339.
54. Babst BA, Ferrier RA, Gray DW, et al. Jasmonic acid induces rapid changes in carbon transport and partitioning in *Populus*. *New Phytol*. 2005;167(1):63–72.
55. Babst BA, Ferrieri RA, Thorpe MR, Orians CM. Lymantria dispar herbivory induces rapid changes in carbon transport and partitioning in *Populus nigra*. *Entomol Exp Appl*. 2008;128(1):117–125.
56. De Schepper V, Bühler J, Thorpe M, et al. ^{11}C -PET imaging reveals transport dynamics and sectorial plasticity of oak phloem after girdling. *Front Plant Sci*. 2013;4(200):200.
57. Ferrieri AP, Agtuca B, Appel HM, Ferrieri RA, Schultz JC. Temporal changes in allocation and partitioning of new carbon as ^{11}C elicited by simulated herbivory suggest that roots shape above-ground responses in *Arabidopsis*. *Plant Physiol*. 2013;161(2):692–704.
58. Garbout A, Munkholm LJ, Hansen SB, Petersen BM, Munk OL, Pajor R. The use of PET/CT scanning technique for 3D visualization and quantification of real-time soil/plant interactions. *Plant Soil*. 2012;352(1-2):113–127.
59. Hidaka K, Miyoshi Y, Ishii S, et al. Dynamic analysis of photosynthate translocation into strawberry fruits using non-invasive ^{11}C -labeling supported with conventional destructive measurements using ^{13}C -labeling. *Front Plant Sci*. 2019;9:1946.
60. Hubeau M, Mincke J, Vanhove C, Courtyn J, Vandenberghe S, Steppe K. Plant-PET to investigate phloem vulnerability to drought in *Populus tremula* under changing climate regimes. *Tree Physiol*. 2018;39(2):211–221.
61. Hubeau M, Thorpe MR, Mincke J, et al. High-resolution *in vivo* imaging of xylem-transported CO_2 in leaves based on real-time ^{11}C -tracing. *Front For Glob Change*. 2019;2:25.
62. Karve AA, Alexoff D, Kim D, Schueller MJ, Ferrieri RA, Babst BA. In vivo quantitative imaging of photoassimilate transport dynamics and allocation in large plants using a commercial positron emission tomography (PET) scanner. *BMC Plant Biol*. 2015;15(1):273.
63. Kawachi N, Fujimaki S, Ishii S, Suzui N, Ishioka NS, Matsuhashi S. A new method for parametric imaging of photosynthesis with C-11 carbon dioxide and positron emitting tracer imaging system (PETIS). *IEEE Nucl Sci Symp Conf Rec*. 2006;3:1519–1522.
64. Kawachi N, Kikuchi K, Suzui N, et al. Imaging of carbon translocation to fruit using carbon-11-labeled carbon dioxide and positron emission tomography. *IEEE Trans Nucl Sci*. 2011;58(2):395–399.
65. Kawachi N, Sakamoto K, Ishii S, et al. Kinetic analysis of carbon-11-labeled carbon dioxide for studying photosynthesis in a leaf using positron emitting tracer imaging system. *IEEE Trans Nucl Sci*. 2006;53(5):2991–2997.
66. Kawachi N, Suzui N, Ishii S, et al. Real-time whole-plant imaging of ^{11}C translocation using positron-emitting tracer imaging system. *Nucl Instrum Methods Phys Res A*. 2011;648(Suppl 1):S317–S320.
67. Keutgen AJ, Keutgen N, Matsuhashi S, et al. Input-output analysis of *in vivo* photoassimilate translocation using positron-emitting tracer imaging system (PETIS) data. *J Exp Bot*. 2005;56(415):1419–1425.

68. Kikuchi K, Ishii S, Fujimaki S, et al. Real-time analysis of photoassimilate translocation in intact eggplant fruit using $^{11}\text{CO}_2$ and a positron-emitting tracer imaging system. *J Japan Soc Hort Sci.* 2008;77(2):199–205.
69. Kurita K, Miyoshi Y, Nagao Y, et al. Fruit PET: 3-D imaging of carbon distribution in fruit using OpenPET. *Nucl Instrum Methods Phys Res A.* 2020; 954:161843.
70. Lee S, Kross B, McKisson J, et al. Imaging corn plants with PhytoPET a modular PET system for plant biology. *IEEE Nucl Sci Symp Conf Rec.* 2013. doi:10.1109/NSSMIC.2013.6829796.
71. Matsuhashi S, Fujimaki S, Kawachi N, Sakamoto K, Ishioka NS, Kume T. Quantitative modeling of photoassimilate flow in an intact plant using the positron emitting tracer imaging system (PETIS). *Soil Sci Plant Nutr.* 2005;51(3):417–423.
72. Matsuhashi S, Fujimaki S, Uchida H, Ishioka NS, Kume T. A new visualization technique for the study of the accumulation of photoassimilates in wheat grains using $[^{11}\text{C}]\text{CO}_2$. *Appl Radiat Isot.* 2006;64(4):435–440.
73. Mudgil Y, Karve A, Teixeira PJPL, Jiang K, Tunc-Ozdemir M, Jones AM. Photosynthate regulation of the root system architecture mediated by the heterotrimeric G protein complex in *Arabidopsis*. *Front Plant Sci.* 2016;7:1255.
74. Qu W, Robert CAM, Erb M, et al. Dynamic precision phenotyping reveals mechanism of crop tolerance to root herbivory. *Plant Physiol.* 2016;172(2):776–788.
75. Robert CAM, Ferrieri RA, Schirmer S, et al. Induced carbon reallocation and compensatory growth as root herbivore tolerance mechanisms. *Plant Cell Environ.* 2014;37(11):2613–2622.
76. Song L, Agtuca B, Schueller MJ, Jurisson SS, Stacey G, Ferrieri RA. Relationship between carbon mobilization and root growth measured by carbon-11 tracer in *Arabidopsis* starch mutants. *J Plant Growth Regul.* 2019;38(4):164–179.
77. Suwa R, Fujimaki S, Suzui N, et al. Use of positron-emitting tracer imaging system for measuring the effect of salinity on temporal and spatial distribution of ^{11}C tracer and coupling between source and sink organs. *Plant Sci.* 2008;175(3):210–216.
78. Thorpe MR, Ferrieri AP, Herth MM, Ferrieri RA. ^{11}C -imaging: methyl jasmonate moves in both phloem and xylem, promotes transport of jasmonate, and of photoassimilate even after proton transport is decoupled. *Planta.* 2007;226(2):541–551.
79. Wang Q, Mathews AJ, Li K, et al. A dedicated high-resolution PET imager for plant sciences. *Phys Med Biol.* 2014;59(19):5613–5629.
80. Yamazaki H, Suzui N, Yin YG, et al. Live-imaging evaluation of the efficacy of elevated CO_2 concentration in a closed cultivation system for the improvement of bioproduction in tomato fruits. *Plant Biotechnol.* 2015;32:31–37.
81. Best M, Schueller MJ, Ferrieri RA. Plant cell wall dynamics are regulated by intercellular sugar trafficking. *Int J Plant Stu.* 2018; 1(1):1–12.
82. Hattori E, Uchida H, Harada N, et al. Incorporation and translocation of 2-deoxy-2- $[^{18}\text{F}]$ fluoro-D-glucose in *Sorghum bicolor* (L.) Moench monitored using a planar positron imaging system. *Planta.* 2008;227(5):1181–1186.
83. Leach KA, Tran TM, Slewinski TL, Meeley RB, Braun DM. Sucrose transporter2 contributes to maize growth, development, and crop yield. *J Integr Plant Biol.* 2017;59(6):390–408.
84. Partelová D, Horník M, Lesný J, Rajec P, Kováč P, Hostin S. Imaging and analysis of thin structures using positron emission tomography: thin phantoms and in vivo tobacco leaves study. *Appl Radiat Isot.* 2016;115:87–96.
85. Partelová D, Kuglerová K, Konotop Y, et al. Imaging of photoassimilates transport in plant tissues by positron emission tomography. *Nova Biotechnol Chim.* 2017;16(1):32–41.
86. Partelová D, Uhrovčík J, Lesný J, et al. Application of positron emission tomography and 2- $[^{18}\text{F}]$ fluoro-2-deoxy-D-glucose for visualization and quantification of solute transport in plant tissues. *Chem Pap.* 2014;68(11):1463–1473.
87. Tran TM, Hampton CS, Brossard TW, et al. In vivo transport of three radioactive $[^{18}\text{F}]$ -fluorinated deoxysucrose analogs by the maize sucrose transporter ZnSUT1. *Plant Physiol Biochem.* 2017; 115:1–17.
88. Davis RA, Rippner DA, Hausner SH, Parikh SJ, McElrone AJ, Sutcliffe JL. In vivo tracking of copper-64 radiolabeled nanoparticles in *Lactuca sativa*. *Environ Sci Technol.* 2017;51(21): 12537–12546.
89. Fontanili L, Lancilli C, Suzui N, et al. Kinetic analysis of zinc/cadmium reciprocal competitions suggests a possible Zn-insensitive pathway for root-to-shoot cadmium translocation in rice. *Rice.* 2016;9(1):1–13.
90. Fujimaki S, Suzui N, Ishioka NS, et al. Tracing cadmium from culture to spikelet: noninvasive imaging and quantitative characterization of absorption, transport, and accumulation of cadmium in an intact rice plant. *Plant Physiol.* 2010;152(4): 1796–1806.
91. Hu P, Yin YG, Ishikawa S, et al. Nitrate facilitates cadmium uptake, transport and accumulation in the hyperaccumulator *Sedum plumbizincicola*. *Environ Sci Pollut Res.* 2013;20(9): 6306–6316.
92. Ishikawa S, Suzui N, Ito-Tanabata S, et al. Real-time imaging and analysis of differences in cadmium dynamics in rice cultivars (*Oryza sativa*) using positron-emitting ^{107}Cd tracer. *BMC Plant Biol.* 2011;11(1):172.
93. Nakamura S, Suzui N, Nagasaka T, et al. Application of glutathione to roots selectively inhibits cadmium transport from roots to shoots in oilseed rape. *J Exp Bot.* 2013;64(4):1073–1081.
94. Sugita R, Kobayashi NI, Hirose A, Tanoi K, Nakanishi TM. Evaluation of in vivo detection properties of ^{22}Na , ^{65}Zn , ^{86}Rb , ^{109}Cd and ^{137}Cs in plant tissues using real-time radioisotope imaging system. *Phys Med Biol.* 2014;59(4):837–851.
95. Tham LX, Nagasawa N, Matsuhashi S, Ishioka NS, Ito T, Kume T. Effect of radiation-degraded chitosan on plants stressed with vanadium. *Radiat Phys Chem.* 2001;61(2):171–175.
96. Yoshihara T, Suzui N, Ishii S, et al. A kinetic analysis of cadmium accumulation in a Cd hyper-accumulator fern, *Athyrium yokoscense* tobacco plants. *Plant Cell Environ.* 2014;37(5):1086–1096.
97. Housh AB, Matthes MS, Gerheart A, et al. Assessment of a ^{18}F -phenylboronic acid radiotracer for imaging boron in maize. *Int J Mol Sci.* 2020;21(3):976.

98. Kawachi N, Fujimaki S, Sakamoto K, Ishioka NS, Matsuhashi S, Sekimoto H. Analysis of NO_3^- interception of the parasitic angiosperm *Orobanchaceae* spp. using a positron-emitting tracer imaging system and $^{13}\text{NO}_3^-$: a new method for the visualization and quantitative analysis of the NO_3^- interception ratio. *Soil Sci Plant Nutr.* 2008;54(3):408–416.
99. Yin YG, Ishii S, Suzui N, et al. On-line rapid purification of [^{13}N] N_2 gas for visualization of nitrogen fixation and translocation in nodulated soybean. *Appl Radiat Isot.* 2019;151:7–12.
100. Nagasawa N, Mitomo H, Ha PTL, et al. Suppression of Zn stress on barley by irradiated chitosan. 2001. Yasunari M, ed. JAERI-Conf—2001-005. Japan.
101. Metzner R, Thorpe MR, Breuer U, et al. Contrasting dynamics of water and mineral nutrients in stems shown by stable isotope tracers and cryo-SIMS. *Plant Cell Environ.* 2010;33(8):1393–1407.
102. Fatangare A, Svatoš A. Applications of 2-deoxy-2-fluoro-D-glucose (FDG) in plant imaging: past, present and future. *Front Plant Sci.* 2016;7:483.
103. Minchin P. Analysis of tracer profiles in phloem transport. *J Exp Botany.* 1978;29(113):1441–1450.
104. James EK, Baldani JJ. The role of biological nitrogen fixation by non-legumes in the sustainable production of food and biofuels. *Plant Soil.* 2012;356(1-2):1–3.
105. Hurek T, Reinhold-Hurek B, Van Montagu M, Kellenberger E. Root colonization and systemic spreading of *Azoarcus* sp. strain BH72 in grasses. *J Bacteriol.* 1994;176(7):1913–1919.
106. Yanni YG, Rizk RY, Corich V, et al. Natural endophytic association between *Rhizobium leguminosarum* bv. trifolii and rice roots and assessment of its potential to promote rice growth. *Plant Soil.* 1997;194:99–114.
107. James EK, Olivares FL. Infection and colonization of sugar cane and other Gramineous plants by endophytic diazotrophs. *Crit Rev Plant Sci.* 1998;17(1):77–119.
108. Okon Y, Labandera-Gonzalez CA. Agronomic applications of *Azospirillum*: an evaluation of 20 years worldwide field inoculation. *Soil Biol Biochem.* 1994;26(12):1591–1601.
109. Dobbelaere S, Croonenborghs A, Thys A, et al. Responses of agronomically important crops to inoculation with *Azospirillum*. *Func Plant Bio.* 2001;28(9):871–879.
110. Pedraza RO, Bellone CH, Carrizo de Bellone S, Boa Sorte PMF, Teixeira KRDS. *Azospirillum* inoculation and nitrogen fertilization effect on grain yield and on the diversity of endophytic bacteria in the phyllosphere of rice rain fed crop. *Eur J Soil Biol.* 2009;45(1):36–43.
111. Farrar K, Bryant D, Cope-Selby N. Understanding and engineering beneficial plant–microbe interactions: plant growth promotion in energy crops. *Plant Biotechnol J.* 2014;12(9):1193–1206.
112. Kinsella K, Schlyer DJ, Fowler JS, Martinez RJ, Sobecky PA. Evaluation of positron emission tomography as a method to visualize subsurface microbial processes. *J Hazard Mater.* 2012;213-214:498–501.
113. Thorpe CL, Williams HA, Boothman C, Lloyd JR, Morris K. Positron emission tomography to visualize in-situ microbial metabolism in natural sediments. *Appl Radiat Isot.* 2019;144:104–110.
114. Vandehey NT, Northern TR, Brodie EL, O’Neil JP. Noninvasive mapping of photosynthetic heterogeneity in biological soil crusts by positron emission tomography: carbon fixation. *Environ Sci Technol Lett.* 2014;1(10):393–398.
115. Boutchko R, Rayz VL, Vandehey NT, et al. Imaging and modeling of flow in porous media using clinical nuclear emission tomography systems and computational fluid dynamics. *J Appl Geophys.* 2012;76:74–81.
116. Gründig M, Richter M, Seese A, Sabri O. Tomographic radiotracer studies of the spatial distribution of heterogeneous geochemical transport processes. *Appl Geochem.* 2007;22(11):2334–2343.
117. Hu Y, Armstrong RT, Hung T, Lee B, Shikhov I, Mostaghimi P. Analysing flow in rocks by combined positron emission tomography and computed tomography imaging. *Soc Core Anal.* 2017;082:1–9.
118. Khalili A, Basu AJ, Pietrzyk U. Flow visualization in porous media via positron emission tomography. *Phys Fluids.* 1998;10(4):1031–1033.
119. Richter M. Concepts for modeling of heterogeneous flow processes in soil columns on the basis of tomographic radiotracer experiments. In: Deutsche Forschungsgemeinschaft (DFG), ed. *Geochemical Processes: Conceptual Models for Reactive Transport in Soil and Groundwater*. 1st ed. Wiley VCH; 2002:20–38.
120. Kulenkampff J, Stoll M, Gründig M, Mansel A, Lippman-Pipke J, Kersten M. Time-lapse 3D imaging by positron emission tomography of Cu mobilized in a soil column by the herbicide MCPA. *Scientific Reports.* 2018;8(1):7091.
121. Kulenkampff J, Gründig M, Zakhnini A, Lippman-Pipke J. Geoscientific process monitoring with positron emission tomography (GeoPET). *Solid Earth.* 2016;7(4):1217–1231.
122. Bach EM, Williams RJ, Hargreaves SK, Yang F, Hofmockel KS. Greatest soil microbial diversity found in micro-habitats. *Soil Biol Biochem.* 2018;118(C):217–226.
123. Mummey D, Holben W, Six J, Stahl P. Spatial stratification of soil bacterial populations in aggregates of diverse soils. *Microb Ecol.* 2006;51(3):404–411.
124. Sessitsch A, Weilharter A, Gerzabek MH, Kirchmann H, Kandeler E. Microbial population structures in soil particle size fractions of a long-term fertilizer field experiment. *Appl Environ Microbiol.* 2001;67(9):4215–4224.
125. Andersson J, Truong P, Halldin C. In-target produced [^{11}C]methane: increased specific radioactivity. *Appl Radiat Isot.* 2009;67(1):106–110.
126. De Boer JR, Pruim J, Van der Lann BF, et al. L-1- ^{11}C -tyrosine PET in patients with laryngeal carcinomas: comparison of standardized uptake value and protein synthesis rate. *J Nucl Med.* 2003;44(3):341–346.
127. Veronese M, Schmidt KC, Smith CB, Bertoldo A. Use of spectral analysis with iterative filter for voxelwise determination of regional rates of cerebral protein synthesis with L-[1- ^{11}C]leucine PET. *J Cereb Blood Flow Metab.* 2012;32(6):1073–1085.
128. Hess E, Sichler S, Kluge A, Coenen HH. Synthesis of 2-[^{18}F]fluoro-L-tyrosine via regiospecific fluoro-de-stannylation. *Appl Radiat Isot.* 2002;57(2):185–191.

129. Saji H, Tanaka A, Magata Y, et al. Procurement and biological significance of pure ^{11}C -glucose. *Radioisotopes*. 1984;33(10): 680–685.
130. Rosen MA, Jones RM, Yano Y, Budinger TF. Carbon-11 choline: synthesis, purification, and brain uptake inhibition by 2-dimethylaminoethanol. *J Nucl Med*. 1985;26(12):1424–1428.
131. Hara T, Iio M, Izuchi R, Tsukiyama T, Yokoi F. Synthesis of pyruvate-1- ^{11}C as a radiopharmaceutical for tumor imaging. *Eur J Nucl Med*. 1985;11(6-7):275–278.
132. McQuade P, McCarthy DW, Welch MJ. Metal radionuclides for PET imaging. In: Valk PE, Bailey DL, Townsend DW, Maisey MN, eds. *Positron Emission Tomography*. 1st ed. Springer-Verlag; 2003:237–250.
133. Wuest F, Berndt M, Kniess T. Carbon-11 labeling chemistry based upon ^{11}C methyl iodide. *Ernst Schering Res Found Workshop*. 2007;(62):183–213.
134. Rotstein BH, Stephenson NA, Vasdev N, Liang SH. Spirocyclic hypervalent iodine(III)-mediated radiofluorination of non-activated and hindered aromatics. *Nat Commun*. 2014;5: 4365.
135. Cascini GL, Asabella AN, Notaristefano A, et al. ^{124}I iodine: a longer-life positron emitter isotope-new opportunities in molecular imaging. *BioMed Res Int*. 2014;(1):672094.
136. Waller S, Wilder SL, Schueller MJ, Housh AB, Ferrieri RA. Quantifying plant-borne carbon assimilation by root-associated bacteria. *Microorganisms*. 2020;8(5):700.
137. Parikh SJ, Goyne KW, Margenot AJ, Mukome FND, Calderón FJ. Soil chemical insights provided through vibrational spectroscopy. *Adv Agron*. 2014;126:1–148.
138. Stuckey JW, Yang J, Wang J, Sparks DL. Advances in scanning transmission X-ray microscopy for elucidating soil biogeochemical processes at the submicron scale. *J Environ Qual*. 2017; 46(6):1166–1174.
139. Mueller CW, Weber PK, Kilburn MR, Hoeschen C, Kleber M, Pett-Ridge J. Advances in the analysis of biogeochemical interfaces: nanoSIMS to investigate soil microenvironments. *Adv Agron*. 2013;121:1–45.
140. Mayali X. NanoSIMS: microscale quantification of biogeochemical activity with large-scale impacts. *Annu Rev Mar Sci*. 2020;12:449–467.
141. Nuñez J, Renslow R, Cliff JB III, Anderton CR. NanoSIMS for biological applications: current practices and analyses. *Biointerfaces*. 2017;13(3):03B301.
142. Bartels B, Svatoš A. Spatially resolved *in vivo* plant metabolomics by laser ablation-based mass spectrometry imaging (MSI) techniques: LDI-MSI and LAESI. *Front Plant Sci*. 2015;6:471.